Dark Energy and the Accelerating Universe

Joshua A. Frieman,[1,2] Michael S. Turner,[2] and Dragan Huterer[3]

[1]Center for Particle Astrophysics, Fermi National Accelerator Laboratory, Batavia, Illinois 60510; email: frieman@fnal.gov

[2]Kavli Institute for Cosmological Physics, The University of Chicago, Chicago, Illinois 60637; email: mturner@uchicago.edu

[3]Department of Physics, University of Michigan, Ann Arbor, Michigan 48109; email: huterer@umich.edu

Key Words

cosmological constant, cosmology, galaxy clusters, large-scale structure, supernovae, weak gravitational lensing

Abstract

Ten years ago, the discovery that the expansion of the universe is accelerating put in place the last major building block of the present cosmological model, in which the universe is composed of 4% baryons, 20% dark matter, and 76% dark energy. At the same time, it posed one of the most profound mysteries in all of science, with deep connections to both astrophysics and particle physics. Cosmic acceleration could arise from the repulsive gravity of dark energy—for example, the quantum energy of the vacuum—or it may signal that general relativity (GR) breaks down on cosmological scales and must be replaced. We review the present observational evidence for cosmic acceleration and what it has revealed about dark energy, discuss the various theoretical ideas that have been proposed to explain acceleration, and describe the key observational probes that will shed light on this enigma in the coming years.

1. INTRODUCTION

In 1998, two teams studying distant type Ia supernovae (SNe Ia) independently presented evidence that the expansion of the universe is speeding up (Riess et al. 1998, Perlmutter et al. 1999). Since Hubble, cosmologists had been trying to measure the slowing of the expansion due to gravity; so certain were they of slow-down that they termed the parameter used to quantify the second derivative of the expansion, q_0, the deceleration parameter (Sandage 1962). The discovery of cosmic acceleration is arguably one of the most important developments in modern cosmology.

The ready acceptance of the supernova results was not a foregone conclusion. The cosmological constant, the simplest explanation of accelerated expansion, had a checkered history, having been invoked and subsequently withdrawn several times before. Since 1998, however, subsequent observations—including more detailed studies of supernovae and independent evidence from clusters of galaxies, large-scale structure (LSS) and the cosmic microwave background (CMB)—have confirmed and firmly established this remarkable finding.

The physical origin of cosmic acceleration remains a deep mystery. According to the theory of general relativity (GR), if the universe is filled with ordinary matter or radiation, the two known constituents of the universe, then gravity should lead to a slowing of the expansion. Because the expansion is speeding up, we are faced with two possibilities, either of which would have profound implications for our understanding of the cosmos and of the laws of physics. The first is that 75% of the energy density of the universe exists in a new form with large negative pressure, known as dark energy. The other possibility is that GR breaks down on cosmological scales and must be replaced with a more complete theory of gravity.

Through a tangled history, dark energy is tied to Einstein's cosmological constant, Λ. Einstein introduced Λ into the field equations of GR in order to produce a static, finite cosmological model (Einstein 1917). With the discovery of the expansion of the universe, the rationale for the cosmological constant evaporated. Fifty years later, Zel'dovich (1968) realized that Λ, mathematically equivalent to the stress energy of empty space, the vacuum, cannot simply be dismissed. In quantum field theory, the vacuum state is filled with virtual particles, and their effects have been measured in the shifts of atomic lines and in particle masses. However, estimates for the energy density associated with the quantum vacuum are at least 60 orders of magnitude too large and are in some cases infinite, a major embarrassment known as the cosmological constant problem (Weinberg 1989).

Despite the troubled history of Λ, the observational evidence for cosmic acceleration was quickly embraced by cosmologists because it provided the missing element needed to complete the current cosmological model. In this model, the universe is spatially flat and is accelerating; is composed of baryons, dark matter, and dark energy; underwent a hot, dense, early phase of expansion that produced the light elements via big bang nucleosynthesis and the CMB; and experienced a much earlier epoch of accelerated expansion, known as inflation, which produced density perturbations from quantum fluctuations, leaving an imprint on the CMB anisotropy and leading by gravitational instability to the formation of LSS.

The current cosmological model also raises deep issues, including the origin of the expansion and the nature of dark matter, as well as the genesis of baryons and the cause of accelerated expansion. Of all these issues, the mystery of cosmic acceleration may be the richest, with broad connections to other important questions in cosmology and in particle physics. For example, the destiny of the universe is tied to understanding dark energy, primordial inflation also involves accelerated expansion and its cause may be related, dark matter and dark energy could be linked, cosmic acceleration could provide a key to finding a successor to Einstein's theory of gravity, the smallness of the energy density of the quantum vacuum might be related to supersymmetry or

even superstring theory, and the cause of cosmic acceleration could give rise to new long-range forces or could be related to the smallness of neutrino masses.

This review is organized into three parts. The first part is devoted to context: In Section 2 we briefly review the Friedmann-Robertson-Walker (FRW) cosmology, the framework for understanding how observational probes of dark energy work. In Section 3 we provide the historical context, from Einstein's introduction of the cosmological constant to the supernova discovery. The second part covers the current status of the field: In Section 4 we review the web of observational evidence that firmly establishes accelerated expansion. In Section 5 we summarize current theoretical approaches to accelerated expansion and dark energy, including the cosmological constant problem, models of dark energy, and modified gravity. In Section 6 we focus on different phenomenological descriptions of dark energy and their relative merits. The third part of the review addresses the future: In Section 7 we discuss the observational techniques that will be used to probe dark energy, primarily supernovae, weak lensing, LSS, and clusters. In Section 8 we describe specific projects aimed at constraining dark energy planned for the next 15 years that have the potential to provide insights into the origin of cosmic acceleration. The connection between the future of the universe and dark energy is the topic of Section 9. In Section 10 we present a summary, framing the two big questions about cosmic acceleration in which progress should be made in the next 15 years—Is dark energy something other than vacuum energy? Does general relativity self-consistently describe cosmic acceleration?—and discussing what we believe are the most important open issues.

Our goal is to broadly review cosmic acceleration for the astronomy community. A number of useful reviews target different aspects of the subject, including theory (Copeland, Sami & Tsujikawa 2006, Padmanabhan 2003), cosmology (Peebles & Ratra 2003), the physics of cosmic acceleration (Uzan 2007), probes of dark energy (Huterer & Turner 2001), dark energy reconstruction (Sahni & Starobinsky 2006), dynamics of dark energy models (Linder 2007), the cosmological constant (Carroll 2001, Carroll, Press & Turner 1992), and the cosmological constant problem (Weinberg 1989).

2. BASIC COSMOLOGY

In this section, we provide a brief review of the elements of the FRW cosmological model. This model provides the context for interpreting the observational evidence for cosmic acceleration as well as the framework for understanding how future cosmological probes will help uncover the cause of acceleration by determining the history of the cosmic expansion with greater precision. For further details on basic cosmology, see, e.g., the textbooks of Dodelson (2003), Kolb & Turner (1990), Peacock (1999), and Peebles (1993). Note that we follow the standard practice of using units in which the speed of light $c = 1$.

2.1. Friedmann-Robertson-Walker Cosmology

From the large-scale distribution of galaxies and the near-uniformity of the CMB temperature, we have good evidence that the universe is nearly homogeneous and isotropic. Under this assumption, the space-time metric can be written in the FRW form,

$$ds^2 = dt^2 - a^2(t)\left[dr^2/(1 - kr^2) + r^2 d\theta^2 + r^2 \sin^2\theta d\phi^2\right], \qquad (1)$$

where r, θ, ϕ are comoving spatial coordinates and t is time, and where the expansion is described by the cosmic scale factor, $a(t)$ (by convention, $a = 1$ today). The quantity k is the curvature of

three-dimensional space: $k = 0$ corresponds to a spatially flat, Euclidean universe, $k > 0$ to positive curvature (three-sphere), and $k < 0$ to negative curvature (saddle).

The wavelengths λ of photons moving through the universe scale with $a(t)$, and the redshift of light emitted from a distant source at time t_{em}, $1 + z = \lambda_{obs}/\lambda_{em} = 1/a(t_{em})$, directly reveals the relative size of the universe at that time. This means that time intervals are related to redshift intervals by $dt = -dz/H(z)(1 + z)$, where $H \equiv \dot{a}/a$ is the Hubble parameter, and the overdot denotes a time derivative. The present value of the Hubble parameter is conventionally expressed as $H_0 = 100\,h$ km/sec/Mpc, where $h \approx 0.7$ is the dimensionless Hubble parameter. Here and below, a subscript 0 on a parameter denotes its value at the present epoch.

The key equations of cosmology are the Friedmann equations, the field equations of GR applied to the FRW metric:

$$H^2 = \left(\frac{\dot{a}}{a}\right)^2 = \frac{8\pi G\rho}{3} - \frac{k}{a^2} + \frac{\Lambda}{3}, \qquad (2)$$

$$\frac{\ddot{a}}{a} = -\frac{4\pi G}{3}(\rho + 3p) + \frac{\Lambda}{3}, \qquad (3)$$

where ρ is the total energy density of the universe (the sum of matter, radiation, dark energy), and p is the total pressure (the sum of the pressures of each component). For historical reasons we display the cosmological constant Λ here. Hereafter, we represent it as vacuum energy and subsume it into the density and pressure terms; the correspondence is $\Lambda = 8\pi G\rho_{VAC} = -8\pi G p_{VAC}$.

For each component, the conservation of energy is expressed by $d(a^3\rho_i) = -p_i\,da^3$, the expanding universe analog of the first law of thermodynamics, $dE = -pdV$. Thus, the evolution of energy density is controlled by the ratio of the pressure to the energy density, the equation-of-state parameter, $w_i \equiv p_i/\rho_i$.[1] For the general case, this ratio varies with time, and the evolution of the energy density in a given component is given by

$$\rho_i \propto \exp\left[3\int_0^z [1 + w_i(z')]d\ln(1 + z')\right]. \qquad (4)$$

In the case of constant w_i,

$$w_i \equiv \frac{p_i}{\rho_i} = \text{constant}, \quad \rho_i \propto (1 + z)^{3(1+w_i)}. \qquad (5)$$

For nonrelativistic matter, which includes both dark matter and baryons, $w_M = 0$ to very good approximation, and $\rho_M \propto (1 + z)^3$; for radiation, i.e., relativistic particles, $w_R = \frac{1}{3}$, and $\rho_R \propto (1+z)^4$. For vacuum energy, as noted above $p_{VAC} = -\rho_{VAC} = -\Lambda/8\pi G = \text{constant}$, i.e., $w_{VAC} = -1$. For other models of dark energy, w can differ from -1 and can vary in time. (Hereafter, w without a subscript refers to dark energy.)

The present energy density of a flat universe ($k = 0$), $\rho_{crit} \equiv 3H_0^2/8\pi G = 1.88 \times 10^{-29}\,h^2$ gm cm^{-3} $= 8.10 \times 10^{-47}\,h^2$ GeV^4, is known as the critical density. It provides a convenient means of normalizing cosmic energy densities, where $\Omega_i = \rho_i(t_0)/\rho_{crit}$. For a positively curved universe $\Omega_0 \equiv \rho(t_0)/\rho_{crit} > 1$, and for a negatively curved universe $\Omega_0 < 1$. The present value of the curvature radius, $R_{curv} \equiv a/\sqrt{|k|}$, is related to Ω_0 and H_0 by $R_{curv} = H_0^{-1}/\sqrt{|\Omega_0 - 1|}$, and the characteristic scale $H_0^{-1} \approx 3000\,h^{-1}$ Mpc is known as the Hubble radius. Because of the

---

[1]A perfect fluid is fully characterized by its isotropic pressure p and its energy density ρ, where p is a function of density and other state variables (e.g., temperature). The equation-of-state parameter $w = p/\rho$ determines the evolution of the energy density ρ; e.g., $\rho \propto V^{-(1+w)}$ for constant w, where V is the volume occupied by the fluid. Vacuum energy or a homogeneous scalar field is spatially uniform and can be fully characterized by w. The evolution of an inhomogeneous, imperfect fluid is in general complicated and is not fully described by w. Nonetheless, in the FRW cosmology, spatial homogeneity and isotropy require the stress energy to take the perfect-fluid form; thus, w determines the evolution of the energy density.
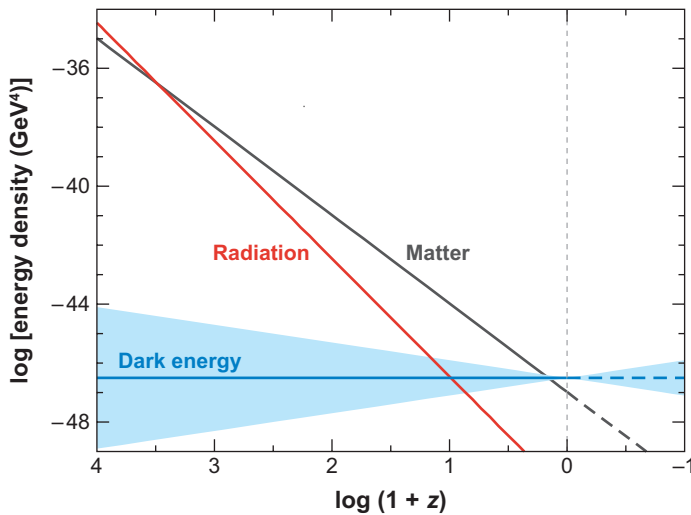
Figure 1

Evolution of radiation, matter, and dark energy densities with redshift. For dark energy, the band represents $w = -1 \pm 0.2$.

evidence from the CMB that the universe is nearly spatially flat (see Section 4.1), we assume $k = 0$ except where otherwise noted.

Figure 1 shows the evolution of the radiation, matter, and dark energy densities with redshift. The universe has gone through three distinct eras: radiation dominated, $z \geq 3000$; matter dominated, $3000 \geq z \geq 0.5$; and dark energy dominated, $z \leq 0.5$. The evolution of the scale factor is controlled by the dominant energy form: $a(t) \propto t^{2/3(1+w)}$ (for constant w). During the radiation-dominated era, $a(t) \propto t^{1/2}$; during the matter-dominated era, $a(t) \propto t^{2/3}$; and during the dark energy–dominated era, assuming $w = -1$, asymptotically $a(t) \propto \exp(Ht)$. For a flat universe with matter and vacuum energy, the general solution—which approaches the latter two above at early and late times—is $a(t) = (\Omega_M/\Omega_{VAC})^{1/3}(\sinh[3\sqrt{\Omega_{VAC}}H_0 t/2])^{2/3}$.

The deceleration parameter, $q(z)$, is defined as

$$q(z) \equiv -\frac{\ddot{a}}{aH^2} = \frac{1}{2}\sum_i \Omega_i(z)\left[1 + 3w_i(z)\right], \tag{6}$$

where $\Omega_i(z) \equiv \rho_i(z)/\rho_{crit}(z)$ is the fraction of critical density in component i at redshift z. During the matter- and radiation-dominated eras $w_i > 0$, and gravity slows the expansion, so that $q > 0$ and $\ddot{a} < 0$. Because of the $(\rho + 3p)$ term in the second Friedmann equation (Newtonian cosmology would only have ρ), the gravity of a component that satisfies $p < -(\rho/3)$, i.e., $w < -(1/3)$, is repulsive and can cause the expansion to accelerate ($\ddot{a} > 0$). We take this to be the defining property of dark energy. The successful predictions of the radiation-dominated era of cosmology, e.g., big bang nucleosynthesis and the formation of CMB anisotropies, provide evidence for the $(\rho + 3p)$ term, as during this epoch $\ddot{a}$ is about twice as large as it would be in Newtonian cosmology.

2.2. Distances and the Hubble Diagram

For an object of intrinsic luminosity L, the measured energy flux F defines the luminosity distance d_L to the object, i.e., the distance inferred from the inverse-square law. The luminosity distance
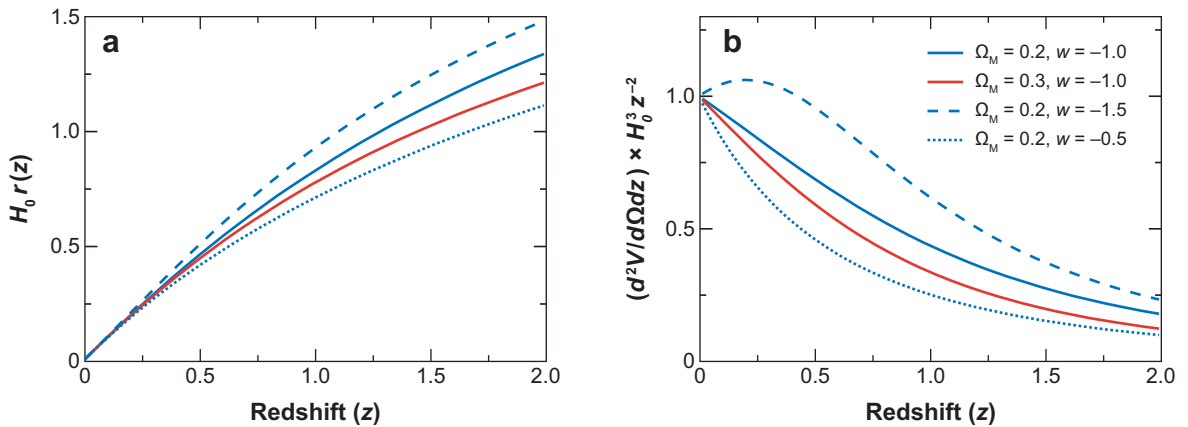
Figure 2

For a flat universe, the effects of dark energy upon cosmic distance (*a*) and upon volume element (*b*) are controlled by Ω_M and w.

is related to the cosmological model through

$$d_L(z) \equiv \sqrt{\frac{L}{4\pi F}} = (1+z)r(z),$$ (7)

where $r(z)$ is the comoving distance to an object at redshift z,

$$r(z) = \int_0^z \frac{dz'}{H(z')} = \int_{1/(1+z)}^1 \frac{da}{a^2 H(a)} \quad (k = 0),$$ (8)

$$r(z) = |k|^{-1/2} \chi \left[|k|^{1/2} \int_0^z dz'/H(z') \right] \quad (k \neq 0),$$ (9)

and where $\chi(x) = \sin(x)$ for $k > 0$ and $\sinh(x)$ for $k < 0$. Specializing to the flat model and constant w,

$$r(z) = \frac{1}{H_0} \int_0^z \frac{dz'}{\sqrt{\Omega_M(1+z')^3 + (1-\Omega_M)(1+z')^{3(1+w)} + \Omega_R(1+z')^4}},$$ (10)

where Ω_M is the present fraction of critical density in nonrelativistic matter, and where $\Omega_R \simeq 0.8 \times 10^{-4}$ represents the small contribution to the present energy density from photons and relativistic neutrinos. In this model, the dependence of cosmic distances upon dark energy is controlled by the parameters Ω_M and w and is shown in **Figure 2a**.

The luminosity distance is related to the distance modulus μ by

$$\mu(z) \equiv m - M = 5 \log_{10} \left(d_L/10 \text{ pc} \right) = 5 \log_{10} \left[(1+z)r(z)/\text{pc} \right] - 5,$$ (11)

where m is the apparent magnitude of the object (proportional to the log of the flux) and where M is the absolute magnitude (proportional to the log of the intrinsic luminosity). Standard candles, objects of fixed absolute magnitude M, and measurements of the logarithmic energy flux m constrain the cosmological model and thereby the expansion history through this magnitude-redshift relation, known as the Hubble diagram.

Expanding the scale factor around its value today, $a(t) = 1 + H_0(t - t_0) - q_0 H_0^2(t - t_0)^2/2 + \cdots$, the distance-redshift relation can be written in its historical form:

$$H_0 d_L = z + \frac{1}{2}(1 - q_0)z^2 + \cdots.$$ (12)

The expansion rate and the present deceleration rate appear in the first two terms in the Taylor expansion of the relation. This expansion, only valid for $z \ll 1$, is of historical significance and utility; it is not useful today, because objects as distant as redshift $z \sim 2$ are being used to probe the expansion history. However, it does illustrate the general principle: The first term on the right-hand side represents the linear Hubble expansion, and the deviation from a linear relation reveals the deceleration (or acceleration).

The angular-diameter distance d_A, the distance inferred from the angular size $\delta\theta$ of a distant object of fixed diameter D, is defined by $d_A \equiv D/\delta\theta = r(z)/(1 + z) = d_L/(1 + z)^2$. The use of standard rulers, objects of fixed intrinsic size, provides another means of probing the expansion history, again through $r(z)$.

The cosmological time, or time back to the Big Bang, is given by

$$t(z) = \int_0^{t(z)} dt' = \int_z^\infty \frac{dz'}{(1 + z')H(z')}. \tag{13}$$

Although the present age in principle depends upon the expansion rate at very early times, the rapid rise of $H(z)$ with z—a factor of 30,000 between today and the epoch of last scattering, when photons and baryons decoupled, at $z_{LS} \simeq 1100$ and $t(z_{LS}) \simeq 380,000$ years—makes this point moot.

Finally, the comoving volume element per unit solid angle $d\Omega$ is given by

$$\frac{d^2V}{dzd\Omega} = r^2 \frac{dr}{dz} \frac{1}{\sqrt{1 - kr^2}} = \frac{r^2(z)}{H(z)}. \tag{14}$$

For a set of objects of known comoving density $n(z)$, the comoving volume element can be used to infer $r^2(z)/H(z)$ from the number counts per unit redshift and solid angle, $d^2N/dzd\Omega = n(z)d^2V/dzd\Omega$. The dependence of the comoving volume element upon Ω_M and w is shown in **Figure 2b**.

2.3. Growth of Structure

A striking success of the consensus cosmology is its ability to account for the observed structure in the universe, provided that dark matter is composed of slowly moving particles, known as cold dark matter (CDM), and that the initial power spectrum of density perturbations is nearly scale invariant, $P(k) \sim k^{n_S}$ with spectral index $n_S \simeq 1$, as predicted by inflation (Springel, Frenk & White 2006). Dark energy affects the development of structure by its influence on the expansion rate of the universe when density perturbations are growing. This fact and the quantity and quality of LSS data make structure formation a sensitive probe of dark energy.

In GR the growth of small-amplitude, matter-density perturbations on length scales much smaller than the Hubble radius is governed by

$$\ddot{\delta}_k + 2H\dot{\delta}_k - 4\pi G\rho_M\delta_k = 0, \tag{15}$$

where the perturbations $\delta(\mathbf{x},\ t) \equiv \delta\rho_M(\mathbf{x}, t)/\bar{\rho}_M(t)$ have been decomposed into their Fourier modes of wave number k, and where matter is assumed to be pressureless (this is always true for the CDM portion and is valid for the baryons on mass scales larger than $10^5\ M_\odot$ after photon-baryon decoupling). Dark energy affects the growth through the "Hubble damping" term, $2H\dot{\delta}_k$.

The solution to Equation 15 is simple to describe for the three epochs of expansion discussed earlier: $\delta_k(t)$ grows as $a(t)$ during the matter-dominated epoch and is approximately constant during the radiation-dominated and dark energy–dominated epochs. Importantly, once accelerated
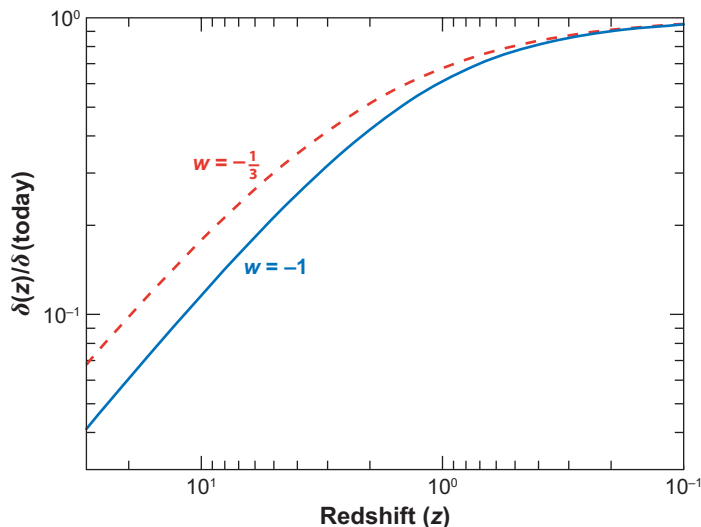
Figure 3

Growth of linear density perturbations in a flat universe with dark energy. Note that the growth of
perturbations ceases when dark energy begins to dominate, $1 + z = (\Omega_{M}/\Omega_{DE})^{1/3w}$.

expansion begins, the growth of linear perturbations effectively ends, as the Hubble damping time
becomes shorter than the timescale for perturbation growth.

The impact of the dark energy equation-of-state parameter w on the growth of structure is
more subtle and is illustrated in **Figure 3**. For larger w and fixed dark energy density Ω_{DE}, dark
energy comes to dominate earlier, causing the growth of linear perturbations to end earlier; this
means that the growth factor since decoupling is smaller and that to achieve the same amplitude
by today, the perturbation must have begun with larger amplitude and must have been larger at
all redshifts until today. The same is true for larger Ω_{DE} and fixed w. Finally, if dark energy is
dynamical (i.e., not vacuum energy), then in principle it can be inhomogeneous, an effect we have
ignored above. In practice, dark energy is expected to be nearly uniform over scales smaller than
the present Hubble radius, in sharp contrast to dark matter, which can clump on small scales.

3. FROM EINSTEIN TO ACCELERATED EXPANSION

Although the discovery of cosmic acceleration is often portrayed as a major surprise and a radical
contravention of the conventional wisdom, it was anticipated by a number of developments in
cosmology during the preceding decade. Moreover, this is not the first time that the cosmological
constant has been proposed. Indeed, the cosmological constant was explored from the very be-
ginnings of GR and has been periodically invoked and subsequently cast aside several times since.
Here we recount some of this complex 90-year history.

3.1. Greatest Blunder?

Einstein introduced the cosmological constant in his field equations in order to obtain a static and
finite cosmological solution "as required by the fact of the small velocities of the stars" and to be
consistent with Mach's principle (Einstein 1917). In Einstein's solution, space is positively curved,
$R_{curv} = 1/\sqrt{4\pi G\rho_{M}}$, and the repulsive gravity of Λ is balanced against the attractive gravity of

matter, $\rho_\Lambda = \rho_M/2$. In 1917, de Sitter explored a solution in which ρ_M is negligible compared to ρ_Λ (de Sitter 1917). There was some early confusion about the interpretation of this model, but in the early 1920s, Weyl, Eddington, and others showed that the apparent recession velocity (the redshift) at small separation would be proportional to the distance, $v = \sqrt{\Lambda/3}\, d$. Also in the 1920s, Friedmann and Lemaître independently showed that cosmological solutions with matter and Λ generally involved expansion or contraction, and Lemaître as well as Eddington showed that Einstein's static solution was unstable to expansion or contraction.

With Hubble's discovery of the expansion of the universe in 1929, Einstein's primary justification for introducing the cosmological constant was lost, and he advocated abandoning it. Gamow (1970) later wrote that Einstein called this "his greatest blunder," as he could have predicted the expanding universe. Yet the description above makes it clear that the history was more complicated, and one could argue that in fact Friedmann and Lemaître (or de Sitter) had predicted the expanding universe, Λ or no. Indeed, Hubble noted that his linear relation between redshift and distance was consistent with the prediction of the de Sitter model (Hubble 1929). Moreover, Eddington recognized that Hubble's value for the expansion rate, $H_0 \simeq 570$ km/s/Mpc, implied a time back to the big bang of less than 2 Gyr, an uncomfortably short time compared to some age estimates of Earth and the Galaxy. By adjusting the cosmological constant to be slightly larger than the Einstein value, $\rho_\Lambda = (1+\varepsilon)\rho_M/2$, a nearly static beginning of arbitrary duration could be obtained, a solution known as the Eddington-Lemaître model. Although Eddington remained focused on Λ, trying to find a place for it in his unified and fundamental theories, most cosmologists abandoned Λ as their major focus.

3.2. Steady State and After

Motivated by the aesthetic beauty of an unchanging universe, Bondi & Gold (1948) and Hoyle (1948) put forth the steady-state cosmology, a revival of the de Sitter model with a new twist. In the steady-state model, the dilution of matter due to expansion is counteracted by postulating the continuous creation of matter ($\sim$1 hydrogen atom per m^3 Gyr^{-1}). However, the model's firm prediction of an unevolving universe made it easily falsifiable, and the redshift distribution of radio galaxies, the absence of quasars nearby, and the discovery of the CMB radiation did so in the early 1960s.

The cosmological constant was briefly resurrected in the late 1960s by Petrosian, Salpeter & Szekeres (1967), who used the Eddington-Lemaître model to explain the preponderance of quasars at redshifts around $z \sim 2$. As it turns out, this is a real observational effect, but it can be attributed to evolution: Quasar activity peaks around this redshift. In 1975, evidence for a cosmological constant from the Hubble diagram of brightest-cluster elliptical galaxies was presented (Gunn & Tinsley 1975), though it was understood (Tinsley & Gunn 1976) that uncertainties in galaxy luminosity evolution make their use as standard candles problematic.

Although cosmologists periodically hauled the cosmological constant out of the closet as needed and then stuffed it back in, in the 1960s physicists began to understand that Λ could not be treated in such a cavalier fashion. With the rise of the standard big bang cosmology came the awareness that Λ could be a big problem. Zel'dovich (1968) realized that the energy density of the quantum vacuum should result in a cosmological constant of enormous size (see Section 5.1.1). However, because of the success of the hot big bang model, the lack of compelling ideas to solve the cosmological constant problem, and the dynamical unimportance of Λ at the early epochs when the hot big bang model was best tested by big bang nucleosynthesis and by the CMB, the problem was largely ignored in cosmological discourse.

3.3. Enter Inflation

In the early 1980s the inflationary universe scenario (Guth 1981), with its predictions of a spatially flat universe ($\Omega = 1$) and almost scale-invariant density perturbations, changed the cosmological landscape and helped set the stage for the discovery of cosmic acceleration. When the idea of inflation was first introduced, the evidence for dark matter was still accruing, and estimates of the total matter density (then about $\Omega_M \sim 0.1$) were sufficiently uncertain that an Einstein–de Sitter model (i.e., $\Omega_M = 1$) could not be ruled out. The evidence for a low value of Ω_M was worrisome enough, however, that some researchers suggested the need for a smooth component, such as vacuum energy, to make up the difference for a flat universe (Peebles 1984; Turner, Steigman & Krauss 1984). Later, the model for structure formation with a cosmological constant and cold dark matter (ΛCDM) and the spectrum of density perturbations predicted by inflation was found to provide a better fit than $\Omega_M = 1$ to the growing observations of LSS (Efstathiou, Sutherland & Maddox 1990; Turner 1991). The 1992 discovery of CMB anisotropy by the Cosmic Background Explorer satellite (COBE) provided the normalization of the spectrum of density perturbations and drove a spike into the heart of the $\Omega_M = 1$ CDM model.

Another important thread in the post-inflation revival of Λ involved age consistency. Although estimates of the Hubble parameter had ranged between 50 and 100 km/s/Mpc since the 1970s, by the mid-1990s they had settled into the middle of that range. Estimates of old globular cluster ages had similar swings, but had settled at $t_0 \simeq 13 - 15$ Gyr. The resulting expansion age, $H_0 t_0 = (H_0/70 \text{ km/s/Mpc})(t_0/14 \text{ Gyr})$, was uncomfortably high compared to that for the Einstein–de Sitter model, for which $H_0 t_0 = \frac{2}{3}$. The cosmological constant offered a ready solution, as the age of a flat universe with Λ rises with Ω_Λ,

$$H_0 t_0 = \frac{1}{3\Omega_\Lambda^{1/2}} \ln\left[\frac{1 + \Omega_\Lambda^{1/2}}{1 - \Omega_\Lambda^{1/2}}\right] = \frac{2}{3}\left[1 + \Omega_\Lambda^2/3 + \Omega_\Lambda^4/5 + \cdots\right], \qquad (16)$$

reaching $H_0 t_0 \simeq 1$ for $\Omega_\Lambda = 0.75$.

By 1995 the cosmological constant was back out of the cosmologists' closet in all its glory (Frieman et al. 1995, Krauss & Turner 1995, Ostriker & Steinhardt 1995): it solved the age problem, it was consistent with growing evidence that $\Omega_M \sim 0.3$, and it fit the growing body of observations of LSS. Its only serious competitors were open inflation, which had a small group of adherents, and hot + cold dark matter, which posited a low value for the Hubble parameter ($\sim$50 km/s/Mpc) and neutrinos accounting for 10% to 15% of the dark matter (see, e.g., contributions in Turok 1997). During the mid-1990s, there were two results that conflicted with ΛCDM: analyses of the statistics of lensed quasars (Kochanek 1996) and of the first seven high-redshift supernovae of the Supernova Cosmology Project (Perlmutter et al. 1997) indicated that $\Omega_\Lambda < 0.66$ and $\Omega_\Lambda < 0.51$ at 95% confidence, respectively, for a flat universe. Ultimately, however, the discovery of accelerated expansion in 1998 saved the theory of inflation by providing evidence for large Ω_Λ.

3.4. Discovery

Two breakthroughs enabled the discovery of cosmic acceleration. The first was the demonstration that SNe Ia are standardizable candles (Phillips 1993). The second was the deployment of large mosaic charge-coupled device (CCD) cameras on 4-m class telescopes, enabling the systematic search of large areas of sky, containing thousands of galaxies, for these rare events. By comparing deep, wide images taken weeks apart, the discovery of supernovae at redshifts $z \sim 0.5$ could be "scheduled" on a statistical basis.
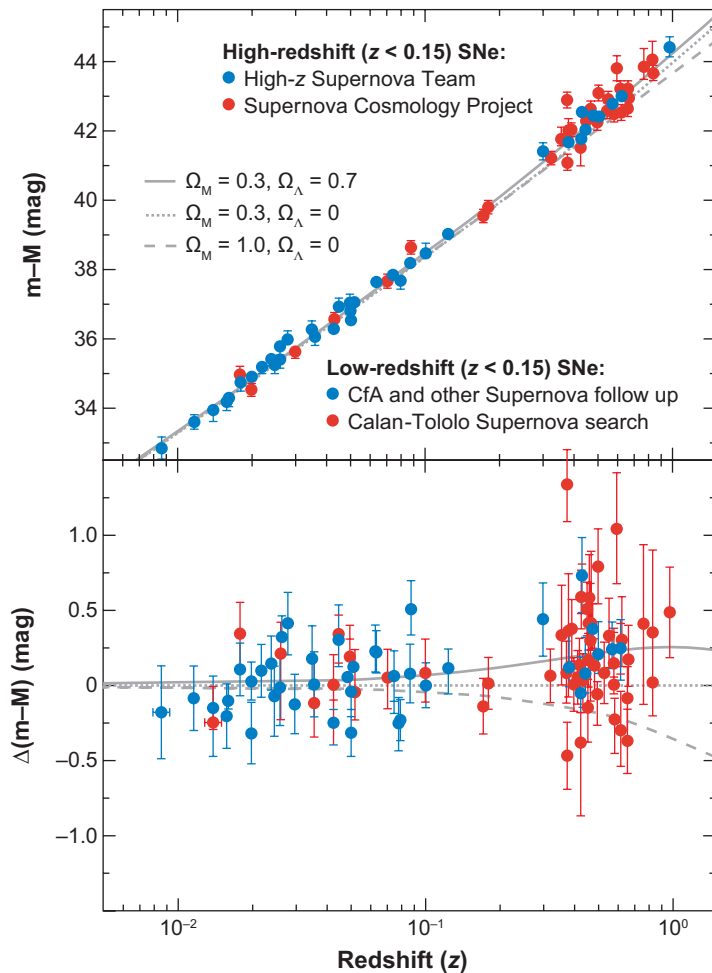
Figure 4

Discovery data: Hubble diagram of type Ia supernovae (SNe Ia) measured by the Supernova Cosmology Project and the High-z Supernova Team. *Bottom*: Residuals in distance modulus relative to an open universe with $\Omega_0 = \Omega_M = 0.3$. Figure adapted from Perlmutter & Schmidt (2003) and Riess (2000), based on Riess et al. (1998) and Perlmutter et al. (1999).

Two teams working independently in the mid- to late 1990s, the Supernova Cosmology Project and the High-z Supernova Search, took advantage of these breakthroughs to measure the supernova Hubble diagram to much larger distances than was previously possible. Both teams found that distant supernovae are ∼0.25 mag dimmer than they would be in a decelerating universe, indicating that the expansion has been speeding up for the past 5 Gyr (Riess et al. 1998, Perlmutter et al. 1999) (see **Figure 4**). When analyzed assuming a universe with matter and cosmological constant, these researchers' results provided evidence for $\Omega_\Lambda > 0$ at greater than 99% confidence (see **Figure 8** for the current constraints).

4. CURRENT STATUS

Since the supernova discoveries were announced in 1998, the evidence for an accelerating universe has become substantially stronger and more broadly based. Subsequent supernova observations have reinforced the original results, and new evidence has accrued from other observational probes. In this section, we review these developments and discuss the current status of the evidence for cosmic acceleration and what we know about dark energy. In Section 7, we address the probes of cosmic acceleration in more detail, and we discuss future experiments in Section 8.

4.1. Cosmic Microwave Background and Large-Scale Structure

Measurements of CMB anisotropy (Jaffe et al. 2001, Pryke et al. 2002) and of LSS provided early and important confirmation of accelerated expansion. The CMB constrains both the amplitude of the primordial fluctuations that give rise to the observed structure and the distance to the last-scattering surface, $r(z \simeq 1100)$. In order to allow sufficient growth of the primordial perturbations and not disrupt the formation of LSS, dark energy must have come to dominate the universe only very recently (see Section 2.3), implying that its energy density evolves with redshift more slowly than matter. This occurs if dark energy has negative pressure, $w < 0$, cf. Equation 5. Likewise, the presence of a component with large negative pressure that accounts for three-quarters of the critical density affects the distance to the last-scattering surface.

4.1.1. Cosmic microwave background. Anisotropies of the CMB provide a record of the universe at a simpler time, before structure had developed and when photons were decoupling from baryons, about 380,000 years after the Big Bang (Hu & Dodelson 2002). The angular power spectrum of CMB temperature anisotropies, measured most recently by the Wilkinson Microwave Anisotropy Probe (WMAP) (Spergel et al. 2007) and by ground-based experiments that probe to smaller angular scales, is dominated by acoustic peaks that arise from gravity-driven sound waves in the photon-baryon fluid (see **Figure 5a**). The positions and amplitudes of the acoustic peaks encode a wealth of cosmological information. They indicate that the universe is nearly spatially flat to within a few percent. In combination with LSS or with independent H_0 measurement, the CMB measurements indicate that matter contributes only about one-quarter of the critical density. A component of missing energy that is smoothly distributed is needed to square these observations, and is fully consistent with the dark energy needed to explain accelerated expansion.

4.1.2. Large-scale structure. Baryon acoustic oscillations (BAO), so prominent in the CMB anisotropy, leave a subtler characteristic signature in the clustering of galaxies, a bump in the two-point correlation function at a scale $\sim 100 \, h^{-1}$ Mpc that can be measured today and that could provide a powerful probe of dark energy in the future (see Section 7.3). Measurement of the BAO signature in the correlation function of Sloan Digital Sky Survey (SDSS) luminous red galaxies (see **Figure 5b**) constrains the distance to redshift $z = 0.35$ to a precision of 5% (Eisenstein et al. 2005). This measurement serves as a significant complement to other probes, as shown in **Figure 8**.

The presence of dark energy affects the large-angle anisotropy of the CMB (the low-ℓ multipoles) through the integrated Sachs-Wolfe (ISW) effect. The ISW arises due to the differential redshifts of photons as they pass through time-changing gravitational potential wells, and it leads to a small correlation between the low-redshift matter distribution and the CMB anisotropy. This effect has been observed in the cross-correlation of the CMB with galaxy and radio source catalogs (Afshordi, Loh & Strauss 2004; Boughn & Crittenden 2004; Fosalba & Gaztanaga 2004; Scranton et al. 2003). This signal indicates that the universe is not described by the Einstein–de Sitter model ($\Omega_M = 1$)—a reassuring cross-check.

Weak gravitational lensing (Munshi et al. 2006, Schneider 2006), the small, correlated distortions of galaxy shapes due to gravitational lensing by intervening LSS, is a powerful technique for mapping dark matter and its clustering. Detection of this cosmic shear signal was first announced by four groups in 2000 (Bacon, Refregier & Ellis 2000; Kaiser, Wilson & Luppino 2000; Van Waerbeke et al. 2000; Wittman et al. 2000). Recent lensing surveys covering areas of order 100 deg^2 have shed light on dark energy by pinning down the combination $\sigma_8(\Omega_M/0.25)^{0.6} \approx 0.85 \pm 0.07$, where σ_8 is the root-mean-square amplitude of mass fluctuations on the $8 \, h^{-1}$ Mpc scale (Hoekstra
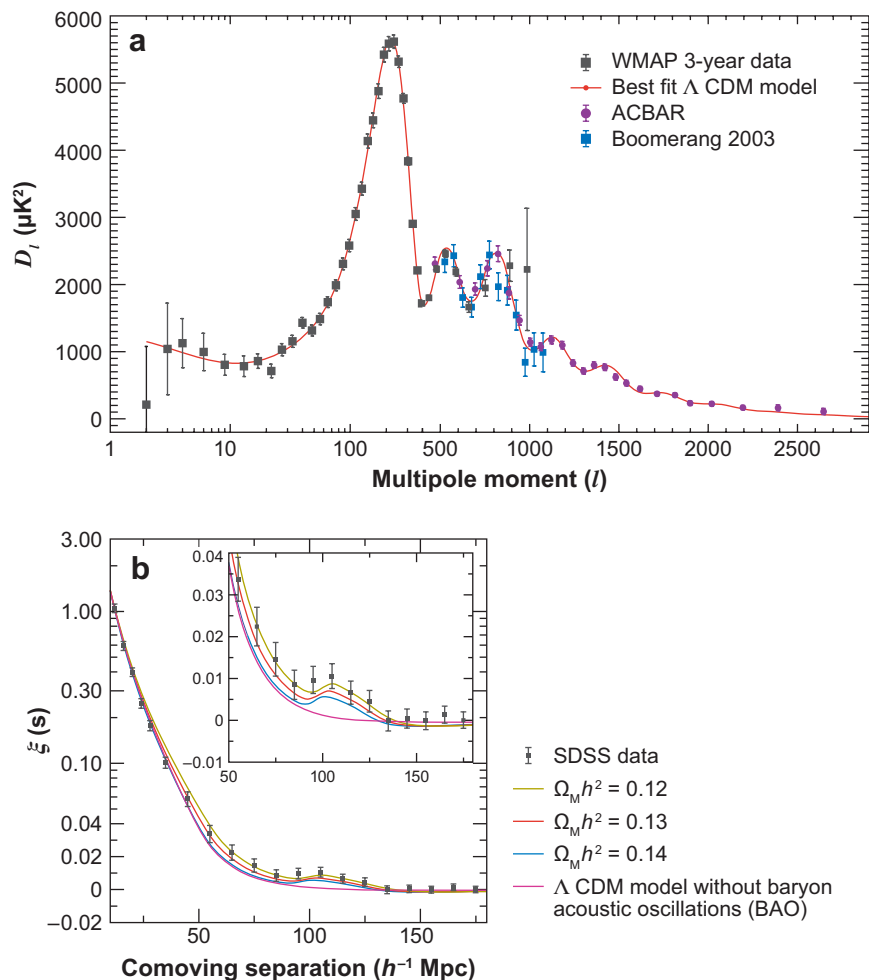
Figure 5

(*a*) Angular power spectrum measurements of the cosmic microwave background temperature fluctuations from the Wilkinson Microwave Anisotropy Probe (WMAP), Boomerang, and the Arcminute Cosmology Bolometer Array Receiver (ACBAR). Data from Reichardt et al. (2008). (*b*) Detection of the baryon acoustic peak in the clustering of luminous red galaxies in the Sloan Digital Sky Survey (Eisenstein et al. 2005). Shown is the two-point galaxy correlation function in redshift space; inset shows an expanded view with a linear vertical axis. Curves correspond to ΛCDM predictions for $\Omega_M h^2 = 0.12$ (*dark yellow*), 0.13 (*red*), and 0.14 (*blue*). The magenta curve shows a ΛCDM model without baryon acoustic oscillations.

et al. 2006, Jarvis et al. 2006, Massey et al. 2007). As other measurements peg σ_8 at $\simeq 0.8$, this implies that $\Omega_M \simeq 0.25$, which is consistent with a flat universe dominated by dark energy. Weak lensing has the potential to be the most powerful probe of dark energy in the future (Hu 2002, Huterer 2002); we discuss this in detail in Sections 7 and 8.

4.2. Recent Supernova Results

A number of concerns were raised about the robustness of the first supernova evidence for acceleration. For instance, it was suggested that distant supernovae could appear fainter due to extinction

by hypothetical gray dust rather than acceleration (Aguirre 1999; Drell, Loredo & Wasserman 2000). Over the intervening decade, the supernova evidence for acceleration has been strengthened by results from a series of supernova surveys. Observations with the Hubble Space Telescope (HST) have provided high-quality light curves (Knop et al. 2003) and have extended supernova measurements to redshift $z \simeq 1.8$, providing evidence for the expected earlier epoch of deceleration and disfavoring dust extinction as an alternative explanation to acceleration (Riess et al. 2001, 2004, 2007). Two large ground-based surveys, the SNLS (Supernova Legacy Survey) (Astier et al. 2006) and the ESSENCE (Equation of State: Supernovae Trace Cosmic Expansion) survey (Miknaitis et al. 2007), have been using 4-m telescopes to measure light curves for several hundred SNe Ia over the redshift range $z \sim 0.3 - 0.9$ with large programs of spectroscopic follow-up on 6- to 10-m telescopes. **Figure 6** shows a compilation of supernova distance measurements from these and other surveys. The quality and quantity of the distant supernova data are now vastly superior to what was available in 1998, and the evidence for acceleration is correspondingly more secure (see **Figure 8**).

4.3. X-Ray Clusters

Measurements of the ratio of X-ray-emitting gas to total mass in galaxy clusters, f_{gas}, also indicate the presence of dark energy. Because clusters are the largest collapsed objects in the universe, the gas fraction in them is presumed to be constant and nearly equal to the baryon fraction in the universe, $f_{gas} \approx \Omega_B / \Omega_M$ (most of the baryons in clusters reside in the gas). The value of f_{gas} inferred from observations depends on the observed X-ray flux and temperature as well as on the distance to the cluster. Only the correct cosmology will produce distances that make the apparent f_{gas} constant in redshift. Using data from the Chandra X-Ray Observatory, Allen et al. (2004, 2007) determined Ω_Λ to a 68% precision of approximately ± 0.2, a value consistent with the supernova data.

4.4. Age of the Universe

Finally, because the expansion age of the universe depends upon the expansion history, the comparison of this age with independent age estimates can be used to probe dark energy. The ages of the oldest stars in globular clusters constrain the age of the universe: $12\,\text{Gyr} \leq t_0 \leq 15\,\text{Gyr}$ (Krauss & Chaboyer 2003). When combined with a weak constraint from structure formation or from dynamical measurements of the matter density, $0.2 < \Omega_M < 0.3$, a consistent age is possible if $-2 \leq w \leq -0.5$ (see **Figure 7**). Age consistency is an important cross-check and provides additional evidence for the defining feature of dark energy, large negative pressure. CMB anisotropy is very sensitive to the expansion age; in combination with LSS measurements, it yields the tight constraint $t_0 = 13.8 \pm 0.2\,\text{Gyr}$ for a flat universe (Tegmark et al. 2006).

4.5. Cosmological Parameters

Sandage (1970) once described cosmology as the quest for two numbers, H_0 and q_0, which were just beyond reach. Today's cosmological model is described by anywhere from 4 to 20 parameters, and the quantity and quality of cosmological data described above enable precise constraints to be placed upon all of them. However, the results depend on which set of parameters are chosen to describe the universe as well as on the types of data used.

For definiteness, we refer to the "consensus" cosmological model (ΛCDM) as one in which k, H_0, Ω_B, Ω_M, Ω_Λ, t_0, σ_8, and n_S are free parameters, but in which dark energy is assumed to be a
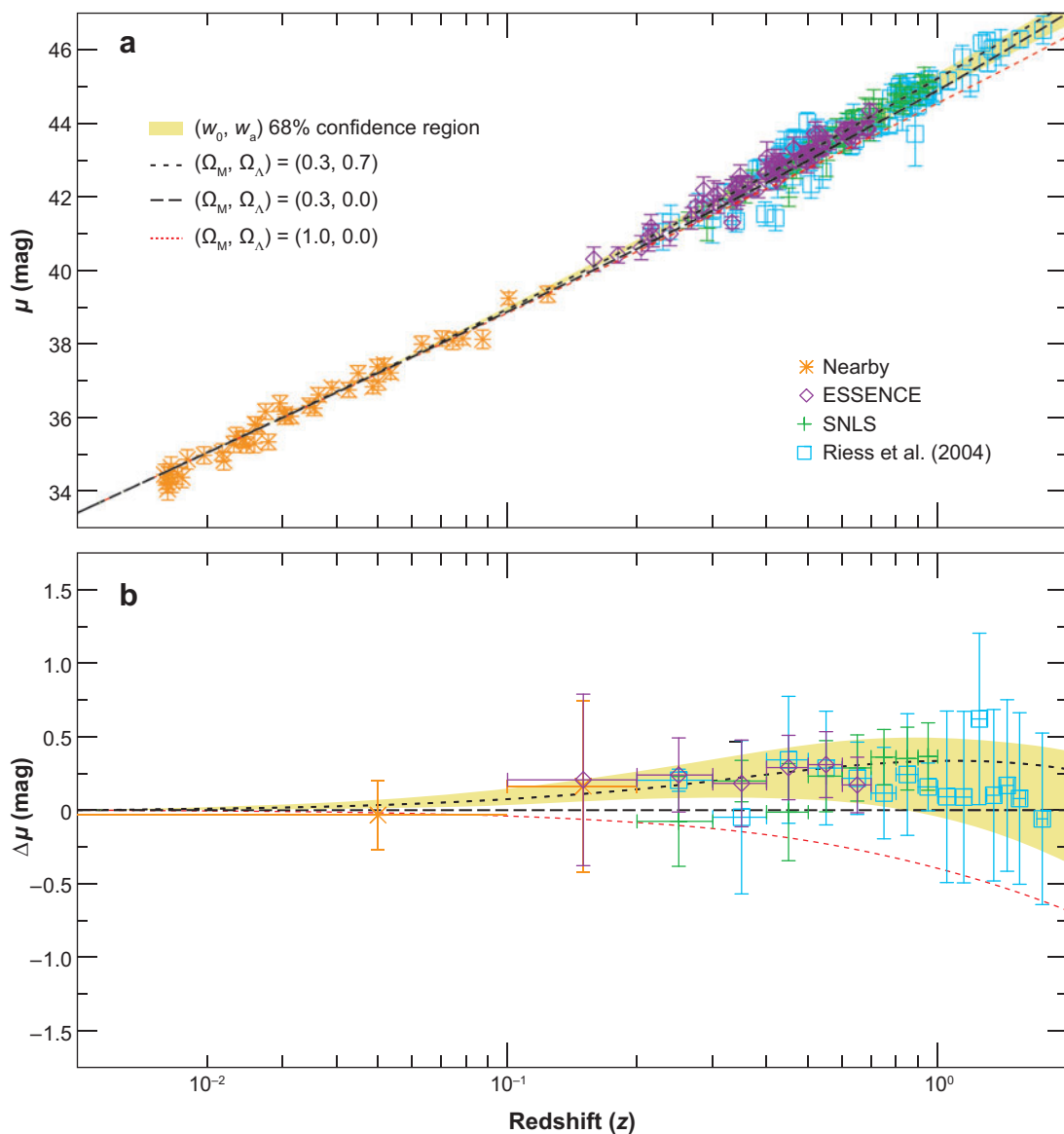
Figure 6

Type Ia supernovae (SNe Ia) results: ESSENCE (Equation of State: Supernovae Trace Cosmic Expansion) (*purple diamonds*), SNLS (Supernova Legacy Survey) (*green crosses*), low-redshift SNe (*orange starbursts*), and the compilation of Riess et al. (2004), which includes many of the other published supernova distances plus those from the *Hubble Space Telescope* (*blue squares*). (*a*) Distance modulus versus redshift (*z*) measurements shown with four cosmological models: $\Omega_M = 0.3$, $\Omega_\Lambda = 0.7$ (*black short-dashed line*); $\Omega_M = 0.3$, $\Omega_\Lambda = 0$ (*black long-dashed line*); $\Omega_M = 1$, $\Omega_\Lambda = 0$ (*red dotted line*); and the 68% CL allowed region in the w_0-w_a plane, assuming spatial flatness and a prior of $\Omega_M = 0.27 \pm 0.03$ (*yellow shading*). (*b*) Binned distance modulus residuals from the $\Omega_M = 0.3$, $\Omega_\Lambda = 0$ model. Adapted from Wood-Vasey et al. (2007).
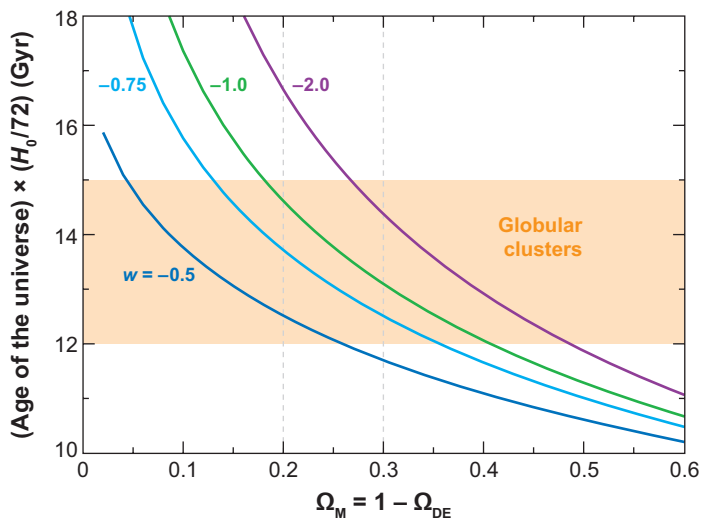
Figure 7

Expansion age of a flat universe versus Ω_M for different values of w. Shown in orange are age constraints
from globular clusters (Krauss & Chaboyer 2003). The vertical dashed lines indicate the favored range for
Ω_M. Age consistency obtains for $-2 \leq w \leq -0.5$.

cosmological constant, $w = -1$. For this model, Tegmark et al. (2006) combined data from SDSS
and WMAP to derive the constraints shown in the second column of **Table 1**.

To both illustrate and gauge the sensitivity of the results to the choice of cosmological param-
eters, we also consider a "fiducial" dark energy model, in which spatial flatness ($k = 0$, $\Omega_0 = 1$)
is imposed and where w is assumed to be a constant that can differ from -1. The cosmological
parameter constraints for this model are given in the third column of **Table 1**.

Although w is not assumed to be -1 in the fiducial model, the data prefer a value that is
consistent with this value, $w = -0.94 \pm 0.1$. Likewise, the data prefer spatial flatness in the
consensus model, in which flatness is not imposed. For the other parameters, the differences are
small. **Figure 8** shows how different data sets individually and in combination constrain parameters

Table 1   Cosmological parameter constraints

Parameter	Consensus model	Fiducial model
Ω_0	1.003 ± 0.010	1 (fixed)
Ω_{DE}	0.757 ± 0.021	0.757 ± 0.020
Ω_M	0.246 ± 0.028	0.243 ± 0.020
Ω_B	0.042 ± 0.002	0.042 ± 0.002
σ_8	0.747 ± 0.046	0.733 ± 0.048
n_S	0.952 ± 0.017	0.950 ± 0.016
H_0 (km/s/Mpc)	72 ± 5	72 ± 3
T_0 (K)	2.725 ± 0.001	2.725 ± 0.001
t_0 (Gyr)	13.9 ± 0.6	13.8 ± 0.2
w	-1 (fixed)	-0.94 ± 0.1
q_0	-0.64 ± 0.03	-0.57 ± 0.1

Data from Tegmark et al. (2006).
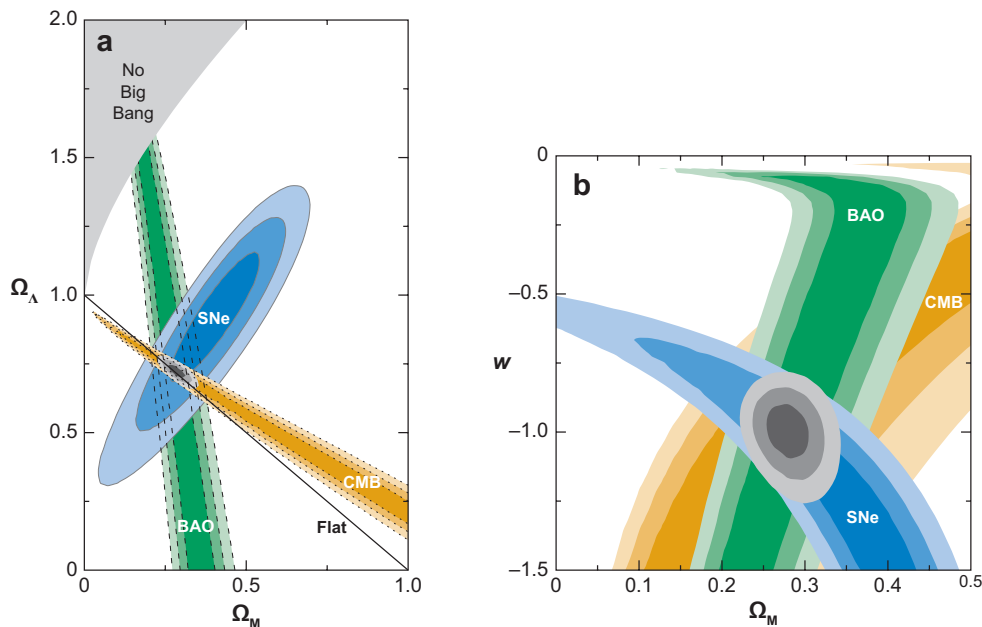
Figure 8

(*a*) Constraints upon Ω_M and Ω_Λ in the consensus model (cosmological constant/cold dark matter model) using baryon acoustic oscillations (BAO), cosmic microwave background (CMB), and supernovae (SNe) measurements. (*b*) Constraints upon Ω_M and constant w in the fiducial dark energy model using the same data sets. Reproduced from Kowalski et al. (2008).

in these two models; although the mix of data used here differs from that in **Table 1** (supernovae are included in **Figure 8**), the resulting constraints are consistent.

Regarding Sandage's two numbers, H_0 and q_0, **Table 1** reflects both good agreement with and a smaller uncertainty than the direct H_0 measurement based upon the extragalactic distance scale, $H_0 = 72 \pm 8$ km/s/Mpc (Freedman et al. 2001). However, the parameter values in **Table 1** are predicated on the correctness of the CDM paradigm for structure formation. The entries for q_0 in **Table 1** are derived from the other parameters using Equation 6. Direct determinations of q_0 require either ultraprecise distances to objects at low redshift or precise distances to objects at moderate redshift. The former are still beyond reach, whereas for the latter the H_0/q_0 expansion is not valid.

If we go beyond the restrictive assumptions of these two models, allowing both curvature and w to be free parameters, then the parameter values shift slightly and the errors increase, as expected. In this case, combining WMAP, SDSS, 2dFGRS (Two-Degree-Field Galaxy Redshift Survey), and SNe Ia data, Spergel et al. (2007) yield $w = -1.08 \pm 0.12$ and $\Omega_0 = 1.026^{+0.016}_{-0.015}$, whereas WMAP + SDSS only bounds H_0 to the range $61 - 84$ km/s/Mpc at 95% confidence (Tegmark et al. 2006), comparable to the accuracy of the HST Key Project measurement (Freedman et al. 2001).

Once we abandon the assumption that $w = -1$, there are no strong theoretical reasons for restricting our attention to constant w. A widely used and simple form that accommodates evolution is $w = w_0 + (1 - a)w_a$ (see Section 6). Future surveys with greater reach than that of present experiments will aim to constrain models in which Ω_M, Ω_{DE}, w_0, and w_a are all free parameters (see Section 8). We note that the current observational constraints on such models are quite
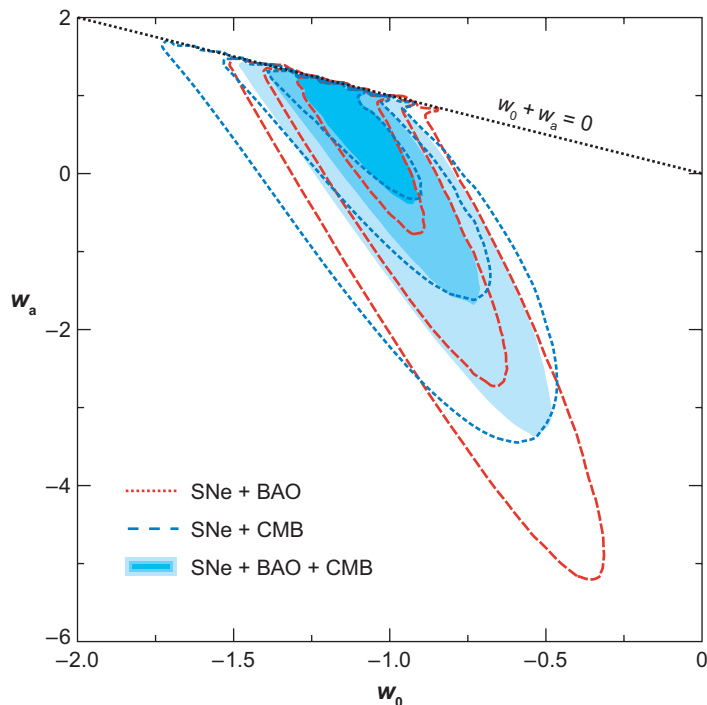
Figure 9

68.3%-, 95.4%-, and 99.7%-CL marginalized constraints on w_0 and w_a in a flat universe, using data from supernovae (SNe), cosmic microwave background (CMB), and baryon acoustic oscillations (BAO). Reproduced from Kowalski et al. (2008).

weak. **Figure 9** shows the marginalized constraints on w_0 and w_a when just three of these four parameters are allowed to vary, using data from the CMB, SNe Ia, and BAO, corresponding to $w_0 \simeq -1 \pm 0.2$, $w_a \sim 0 \pm 1$ (Kowalski et al. 2008). Although the extant data are fully consistent with ΛCDM, they do not exclude more exotic models of dark energy in which the dark energy density or its equation-of-state parameter varies with time.

5. UNDERSTANDING COSMIC ACCELERATION

Understanding the origin of cosmic acceleration presents a stunning opportunity for theorists. As discussed in Section 2, a smooth component with large negative pressure has repulsive gravity and can lead to the observed accelerated expansion within the context of GR. This serves to define dark energy. There is no shortage of ideas for what dark energy might be, ranging from the quantum vacuum to a new, ultralight scalar field. Alternatively, cosmic acceleration may arise from new gravitational physics, perhaps involving extra spatial dimensions. Here, we briefly review the theoretical landscape.

5.1. Dark Energy Models

5.1.1. Vacuum energy. Vacuum energy is simultaneously the most plausible and the most puzzling dark energy candidate. General covariance requires that the stress energy of the vacuum take the form of a constant times the metric tensor, $T_{\mathrm{VAC}}^{\mu\nu} = \rho_{\mathrm{VAC}} g^{\mu\nu}$. Because the diagonal terms

(T_0^0, T_i^i) of the stress-energy tensor T_ν^μ are the energy density and minus the pressure of the fluid, and because g_ν^μ is just the Kronecker delta, the vacuum has a pressure equal to minus its energy density, $p_{VAC} = -\rho_{VAC}$. This also means that vacuum energy is mathematically equivalent to a cosmological constant.

Attempts to compute the value of the vacuum energy density lead to very large or divergent results. For each mode of a quantum field there is a zero-point energy $\hbar\omega/2$, so that the energy density of the quantum vacuum is given by

$$\rho_{VAC} = \frac{1}{2} \sum_{fields} g_i \int_0^\infty \sqrt{k^2 + m^2} \frac{d^3k}{(2\pi)^3} \simeq \sum_{fields} \frac{g_i k_{max}^4}{16\pi^2}, \qquad (17)$$

where g_i accounts for the degrees of freedom of the field (the sign of g_i is + for bosons and − for fermions) and where the sum runs over all quantum fields (e.g., quarks, leptons, gauge fields, etc.). Here k_{max} is an imposed momentum cutoff, because the sum diverges quartically.

To illustrate the magnitude of the problem, if the energy density contributed by just one field is to be at most the critical density, then the cutoff k_{max} must be <0.01 eV—well below any energy scale where one could appeal to ignorance of physics beyond. [Pauli reportedly carried out this calculation in the 1930s, using the electron mass scale for k_{max} and finding that the size of the universe, that is, H^{-1}, "could not even reach to the moon" (Straumann 2002).] Taking the cutoff to be the Planck scale ($\approx 10^{19}$ GeV), where one expects quantum field theory in a classical space-time metric to break down, the zero-point energy density would exceed the critical density by some 120 orders of magnitude! It is very unlikely that a classical contribution to the vacuum energy density would cancel this quantum contribution to such high precision. This very large discrepancy is known as the cosmological constant problem (Weinberg 1989).

Supersymmetry (SUSY), the hypothetical symmetry between bosons and fermions, appears to provide only partial help. In a supersymmetric world, every fermion in the standard model of particle physics has an equal-mass SUSY bosonic partner and vice versa, so that fermionic and bosonic zero-point contributions to ρ_{VAC} would exactly cancel. However, SUSY is not a manifest symmetry in nature: none of the SUSY particles has yet been observed in collider experiments, so they must be substantially heavier than their standard model partners. If SUSY is spontaneously broken at a mass scale M, one would expect the imperfect cancellations to generate a finite vacuum energy density $\rho_{VAC} \sim M^4$. For the currently favored value $M \sim 1$ TeV, this leads to a discrepancy of 60 (as opposed to 120) orders of magnitude with observations. Nonetheless, experiments at the Large Hadron Collider (LHC) at the European Laboratory for Particle Physics (CERN) will soon begin searching for signs of SUSY, e.g., SUSY partners of the quarks and leptons, and may shed light on the vacuum energy problem.

Another approach to the cosmological constant problem involves the idea that the vacuum energy scale is a random variable that can take on different values in different disconnected regions of the universe. Because a value much larger than that needed to explain the observed cosmic acceleration would preclude the formation of galaxies (assuming that all other cosmological parameters are held fixed), we could not exist in a region with such large ρ_{VAC} (Weinberg 1987). This anthropic approach accords well with the landscape version of string theory, in which the number of different vacuum states is very large and in which essentially all values of the cosmological constant are possible. Provided that the universe has such a multiverse structure, this might provide an explanation for the smallness of the cosmological constant (Bousso & Polchinski 2000, Susskind 2003).

5.1.2. Scalar fields. Vacuum energy does not vary with space or time, and it is not dynamical. However, by introducing a new degree of freedom, a scalar field ϕ, one can make vacuum energy
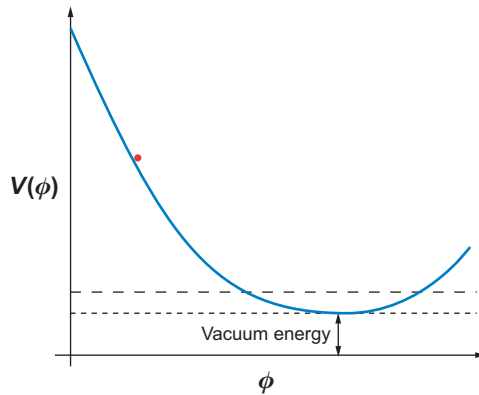
Figure 10

Generic scalar potential $V(\phi)$. The scalar field rolls down the potential, eventually settling at its minimum, which corresponds to the vacuum. The energy associated with the vacuum can be positive, negative, or zero.

effectively dynamical (Wetterich 1988; Ratra & Peebles 1988; Frieman et al. 1995; Zlatev, Wang & Steinhardt 1999). For a scalar field ϕ with Lagrangian density $\mathcal{L} = \frac{1}{2}\partial^\mu\phi\partial_\mu\phi - V(\phi)$, the stress energy takes the form of a perfect fluid, with

$$\rho = \dot{\phi}^2/2 + V(\phi), \quad p = \dot{\phi}^2/2 - V(\phi), \tag{18}$$

where ϕ is assumed to be spatially homogeneous (i.e., $\phi(\vec{x}, t) = \phi(t)$), $\dot{\phi}^2/2$ is the kinetic energy, and $V(\phi)$ is the potential energy (see **Figure 10**). The evolution of the field is governed by its equation of motion,

$$\ddot{\phi} + 3H\dot{\phi} + V'(\phi) = 0, \tag{19}$$

where the prime denotes differentiation with respect to ϕ. Scalar-field dark energy can be described by the equation-of-state parameter

$$w = \frac{\dot{\phi}^2/2 - V(\phi)}{\dot{\phi}^2/2 + V(\phi)} = \frac{-1 + \dot{\phi}^2/2V}{1 + \dot{\phi}^2/2V}. \tag{20}$$

If the scalar field evolves slowly, $\dot{\phi}^2/2V \ll 1$, then $w \approx -1$, and the scalar field behaves like a slowly varying vacuum energy, with $\rho_{\mathrm{VAC}}(t) \simeq V[\phi(t)]$. In general, from Equation 20, w can take on any value between -1 (rolling very slowly) and $+1$ (evolving very rapidly) and varies with time.

Many scalar-field models can be classified dynamically as "thawing" or "freezing" (Caldwell & Linder 2005). In freezing models, the field rolls more slowly as time progresses, i.e., the slope of the potential drops more rapidly than the Hubble friction term $3H\dot{\phi}$ in Equation 19. This can happen if, for instance, $V(\phi)$ falls off exponentially or as an inverse power law at large ϕ. For thawing models, at early times the field is frozen by the friction term and acts as vacuum energy; when the expansion rate drops below $H^2 = V''(\phi)$, the field begins to roll and w evolves away from -1. The simplest example of a thawing model is a scalar field of mass m_ϕ, with $V(\phi) = m_\phi^2\phi^2/2$. Because thawing and freezing fields tend to have different trajectories of $w(z)$, precise cosmological measurements may be able to discriminate between them.

5.1.3. Cosmic coincidence and scalar fields. As **Figure 1** shows, through most of the history of the universe dark matter or radiation dominated dark energy by many orders of magnitude. We happen to live at a time when dark energy has become important. Is this coincidence between ρ_{DE} and ρ_{M} an important clue to understanding cosmic acceleration or just a natural consequence

of the different scalings of cosmic energy densities and the longevity of the universe? In some freezing models, the scalar-field energy density tracks that of the dominant component (radiation or matter) at early times and then dominates at late times, providing a dynamical origin for the coincidence. In thawing models, the coincidence is indeed transitory and merely reflects the mass scale of the scalar field.

5.1.4. More complicated scalar-field models. Although the choice of the potential $V(\phi)$ allows a large range of dynamical behaviors, theorists have also considered the implications of modifying the canonical form of the kinetic energy term $\frac{1}{2}\partial^{\mu}\phi\partial_{\mu}\phi$ in the Lagrangian. By changing the sign of this term, from Equation 20 it is possible to have $w < -1$ (Caldwell 2002), although such theories are typically unstable (Carroll, Hoffman & Trodden 2003). In k-essence, one introduces a field-dependent kinetic term in the Lagrangian to address the coincidence problem (Armendariz-Picon, Mukhanov & Steinhardt 2000).

5.1.5. Scalar-field issues. Scalar-field models raise new questions and possibilities. For example, is cosmic acceleration related to inflation? After all, both phenomena involve accelerated expansion and can be explained by scalar-field dynamics. Is dark energy related to dark matter or to neutrino mass? No firm or compelling connections have been made to either, although the possibilities are intriguing. Unlike vacuum energy, which must be spatially uniform, scalar-field dark energy can clump, providing a possible new observational feature. In most cases, however, it is only expected to do so on the largest observable scales (see Section 10.2.1).

Introducing a new dynamical degree of freedom allows for a richer variety of explanations for cosmic acceleration, but it is not a panacea. Scalar-field models do not address the cosmological constant problem; they simply assume that the minimum value of $V(\phi)$ is very small or zero (see **Figure 10**). Cosmic acceleration is then attributable to the fact that the universe has not yet reached its true vacuum state for dynamical reasons. These models also pose new challenges: In order to roll slowly enough to produce accelerated expansion, the effective mass of the scalar field must be very light compared to other mass scales in particle physics, $m_{\phi} \equiv \sqrt{V''(\phi)} \leq 3H_0 \simeq 10^{-42}$ GeV, even though the field amplitude is typically of order the Planck scale, $\phi \sim 10^{19}$ GeV. This hierarchy, $m_{\phi}/\phi \sim 10^{-60}$, means that the scalar-field potential must be extremely flat. Moreover, in order not to spoil this flatness, the interaction strength of the field with itself must be extremely weak, at most of order 10^{-120} in dimensionless units. Its coupling to matter must also be very weak to be consistent with constraints upon new long-range forces (Carroll 1998). Understanding such small numbers and ratios makes it challenging to connect scalar-field dark energy with particle physics models (Frieman et al. 1995). In constructing theories that go beyond the standard model of particle physics, including those that incorporate primordial inflation, model builders have been guided by the requirement that any small dimensionless numbers in the theory should be protected by symmetries from large quantum corrections (as in the SUSY example given above). Thus far, such model-building discipline has not been the rule among cosmologists working on dark energy models.

5.2. Modified Gravity

A very different approach holds that cosmic acceleration is a manifestation of new gravitational physics rather than dark energy, i.e., that it involves a modification of the geometric as opposed to the stress-tensor side of the Einstein equations. Assuming that four-dimensional space-time can still be described by a metric, the operational changes are twofold: (*a*) a new version of the Friedmann equation governing the evolution of $a(t)$ and (*b*) modifications to the equations that

govern the growth of the density perturbations that evolve into LSS. A number of ideas have been explored along these lines, from models motivated by higher-dimensional theories and string theory (Deffayet 2001; Dvali, Gabadadze & Porrati 2000) to phenomenological modifications of the Einstein-Hilbert Lagrangian of GR (Carroll et al. 2004; Song, Hu & Sawicki 2007).

Changes to the Friedmann equation are easier to derive, discuss, and analyze. In order not to spoil the success of the standard cosmology at early times (from big bang nucleosynthesis to the CMB anisotropy to the formation of structure), the Friedmann equation must reduce to the GR form for $z \gg 1$. As a specific example, consider the model of Dvali, Gabadadze & Porrati (2000), which arises from a five-dimensional gravity theory and has a four-dimensional Friedmann equation,

$$H^2 = \frac{8\pi G\rho}{3} + \frac{H}{r_c}, \tag{21}$$

where r_c is a length scale related to the five-dimensional gravitational constant. As the energy density in matter and radiation, ρ, becomes small, there emerges an accelerating solution, with $H = 1/r_c$. From the viewpoint of expansion, the additional term in the Friedmann equation has the same effect as dark energy that has an equation-of-state parameter that evolves from $w = -1/2$ (for $z \gg 1$) to $w = -1$ in the distant future. Although this approach is attractive, it is not clear that a self-consistent model with this dynamical behavior exists (e.g., Gregory et al. 2007).

5.3. Unmodified Gravity

Instead of modifying the right or left side of the Einstein equations to explain the supernova observations, a third logical possibility is to abandon the assumption that the universe is spatially homogeneous on large scales. It has been argued that the nonlinear gravitational effects of spatial density perturbations, when averaged over large scales, could yield a distance-redshift relation in our observable patch of the universe that is very similar to that for an accelerating, homogeneous universe (Kolb, Matarrese & Riotto 2006), obviating the need for either dark energy or modified gravity. Although there has been debate about the amplitude of these effects, this idea has helped spark renewed interest in a class of exact, inhomogeneous cosmologies. For such Lemaître-Tolman-Bondi models to be consistent with the supernova data and not to conflict with the isotropy of the CMB, the Milky Way must be near the center of a very large scale, nearly spherical, underdense region (Tomita 2001; Alnes, Amarzguioui & Gron 2006; Enqvist 2007). Whether or not such models can be made consistent with the wealth of precision cosmological data remains to be seen; moreover, requiring our Galaxy to occupy a privileged location, in violation of the spirit of the Copernican principle, is not yet theoretically well motivated.

5.4. Theory Summary

There is no compelling explanation for cosmic acceleration, but many intriguing ideas are being explored. Here is our assessment of the ideas described above:

- Cosmological constant: simple, but no underlying physics.
- Vacuum energy: well motivated, mathematically equivalent to a cosmological constant. $w = -1$ is consistent with all data, but all attempts to estimate its size are at best orders of magnitude too large.
- Scalar fields: temporary period of cosmic acceleration, w varies between -1 and 1 (and could also be < -1), possibly related to inflation, but does not address the cosmological constant problem and may lead to new long-range forces.

- New gravitational physics: Cosmic acceleration could be a clue to going beyond GR, but no self-consistent model has been put forth.
- Old gravitational physics: It may be possible to find an inhomogeneous solution that is observationally viable, but such solutions do not yet seem compelling.

The ideas underlying many of these approaches, from attempting to explain the smallness of quantum vacuum energy to extending Einstein's theory, are bold. Solving the puzzle of cosmic acceleration thus has the potential to advance our understanding of many important problems in fundamental physics.

6. DESCRIBING DARK ENERGY

The absence of a consensus model for cosmic acceleration presents a challenge in trying to connect theory with observation. For dark energy, the equation-of-state parameter w provides a useful phenomenological description (Turner & White 1997). Because it is the ratio of pressure to energy density, it is also closely connected to the underlying physics. However, w is not fundamentally a function of redshift, and if cosmic acceleration is due to new gravitational physics, the motivation for a description in terms of w disappears. In this section, we review the variety of formalisms that have been used to describe and constrain dark energy.

6.1. Parameterizations

The simplest parameterization of dark energy is $w = $ const. This form fully describes vacuum energy ($w = -1$) and, together with Ω_{DE} and Ω_M, provides a three-parameter description of the dark energy sector (two parameters if flatness is assumed). However, it does not describe scalar-field or modified-gravity models.

A number of two-parameter descriptions of w have been explored, e.g., $w(z) = w_0 + w'z$ and $w(z) = w_0 + b\ln(1 + z)$. For low redshift they are all essentially equivalent, but for large redshift some lead to unrealistic behavior, e.g., $w \ll -1$ or $\gg 1$. The parameterization

$$w(a) = w_0 + w_a(1 - a) = w_0 + w_a z/(1 + z) \tag{22}$$

(e.g., Linder 2003) avoids this problem and leads to the most commonly used description of dark energy, namely (Ω_{DE}, Ω_M, w_0, w_a).

More general expressions have been proposed, for example, Padé approximants and the transition between two asymptotic values w_0 (at $z \to 0$) and w_f (at $z \to \infty$), $w(z) = w_0 + (w_f - w_0)/(1 + \exp[(z - z_t)/\Delta])$ (Corasaniti & Copeland 2003). The two-parameter descriptions of $w(z)$ that are linear in the parameters entail the existence of a "pivot" redshift z_p, at which the measurements of the two parameters are uncorrelated and where the error in $w_p \equiv w(z_p)$ reaches a minimum (Huterer & Turner 2001) (see **Figure 11a**). The redshift of this sweet spot varies with the cosmological probe and survey specifications; for example, for current SNe Ia surveys $z_p \approx 0.25$. Note that forecast constraints for a particular experiment on w_p are numerically equivalent to constraints one would derive on constant w.

6.2. Direct Reconstruction

Another approach is to directly invert the redshift-distance relation $r(z)$ measured from supernova data to obtain the redshift dependence of $w(z)$ in terms of the first and second derivatives of the
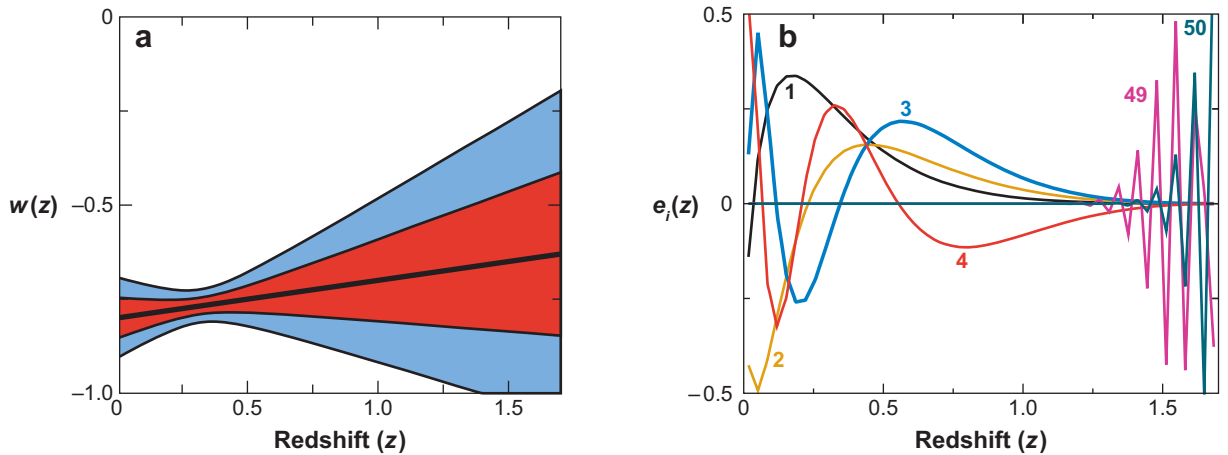
Figure 11

(*a*) Example of forecast constraints on $w(z)$, assuming $w(z) = w_0 + w'z$. The "pivot" redshift, $z_p \approx 0.3$, is where $w(z)$ is best determined. Reproduced from Huterer & Turner (2001). (*b*) The four best-determined (labeled 1–4) and two worst-determined (labeled 49, 50) principal components of $w(z)$ for a future type Ia supernovae (SNe Ia) survey such as the Supernova/Acceleration Probe, with several thousand SNe in the redshift range $z = 0$ to $z = 1.7$. Reproduced from Huterer & Starkman (2003).

comoving distance (Starobinsky 1998, Huterer & Turner 1999, Nakamura & Chiba 1999),

$$1 + w(z) = \frac{1+z}{3} \, \frac{3H_0^2 \Omega_M (1+z)^2 + 2(d^2r/dz^2)/(dr/dz)^3}{H_0^2 \Omega_M (1+z)^3 - (dr/dz)^{-2}}. \tag{23}$$

Assuming that dark energy is due to a single rolling scalar field, the scalar potential can also be reconstructed:

$$V[\phi(z)] = \frac{1}{8\pi G} \left[\frac{3}{(dr/dz)^2} + (1+z)\frac{d^2r/dz^2}{(dr/dz)^3} \right] - \frac{3\Omega_M H_0^2 (1+z)^3}{16\pi G}. \tag{24}$$

Others have suggested reconstructing the dark energy density (Wang & Mukherjee 2004):

$$\rho_{DE}(z) = \frac{3}{8\pi G} \left[\frac{1}{(dr/dz)^2} - \Omega_M H_0^2 (1+z)^3 \right]. \tag{25}$$

Direct reconstruction is the only approach that is truly model independent. However, it comes at a price: taking derivatives of noisy data. In practice, one must fit the distance data with a smooth function, e.g., a polynomial, a Padé approximant, or a spline with tension, and the fitting process introduces systematic biases. Although a variety of methods have been pursued (e.g., Gerke & Efstathiou 2002, Weller & Albrecht 2002), it appears that direct reconstruction is too challenging and not robust enough even with SNe Ia data of excellent quality. Moreover, although the expression for $\rho_{DE}(z)$ involves only first derivatives of $r(z)$, it contains little information about the nature of dark energy. For a review of dark energy reconstruction and related issues, see Sahni & Starobinsky (2006).

6.3. Principal Components

The cosmological function that we are trying to determine—$w(z)$, $\rho_{DE}(z)$, or $H(z)$—can be expanded in terms of principal components, a set of functions that are uncorrelated and orthogonal by construction (Huterer & Starkman 2003). In this approach, the data determine which components are measured best.

For example, suppose we parameterize $w(z)$ in terms of piecewise constant values w_i ($i = 1, \ldots, N$), each defined over a small redshift range ($z_i, z_i + \Delta z$). In the limit of small Δz this procedure recovers the shape of an arbitrary dark energy history (in practice, $N \geq 20$ is sufficient), but the estimates of the w_i from a given dark energy probe will be very noisy for large N. Principal components analysis extracts from those noisy estimates the best-measured features of $w(z)$. We find the eigenvectors $e_i(z)$ of the inverse covariance matrix for the parameters w_i and the corresponding eigenvalues λ_i. The equation-of-state parameter is then expressed as

$$w(z) = \sum_{i=1}^{N} \alpha_i e_i(z), \qquad (26)$$

where the $e_i(z)$ are the principal components. The coefficients α_i, which can be computed via the orthonormality condition, are each determined with an accuracy $1/\sqrt{\lambda_i}$. Several of these components are shown for a future supernova survey in **Figure 11a**.

One can use this approach to design a survey that is the most sensitive to the dark energy equation-of-state parameter in a specific redshift interval or to study how many independent parameters are measured well by a combination of cosmological probes. There are a variety of extensions of this method, including measurements of the equation-of-state parameter in redshift intervals (Huterer & Cooray 2005).

6.4. Kinematic Description

If the explanation of cosmic acceleration is a modification of GR and not dark energy, then a purely kinematic description through, e.g., the functions $a(t)$, $H(z)$, or $q(z)$ may be the best approach. With the weaker assumption that gravity is described by a metric theory and that space-time is isotropic and homogeneous, the FRW metric is still valid, as are the kinematic equations for redshift/scale factor, age, $r(z)$, and volume element. However, the dynamical equations, i.e., the Friedmann equations and the growth of density perturbations, may be modified.

On the one hand, if $H(z)$ is chosen as the kinematic variable, then $r(z)$ and age take their standard forms. On the other hand, to describe acceleration one may wish to take the deceleration parameter $q(z)$ as the fundamental variable; the expansion rate is then given by

$$H(z) = H_0 \exp \left[\int_0^z [1 + q(z')] d \ln(1 + z') \right]. \qquad (27)$$

Another possibility is to use the dimensionless "jerk" parameter, $j \equiv (\dddot{a}/a)/H^3$, instead of $q(z)$ (Visser 2004, Rapetti et al. 2007). The deceleration $q(z)$ can be expressed in terms of $j(z)$,

$$\frac{dq}{d \ln(1 + z)} + q(2q + 1) - j = 0, \qquad (28)$$

and, supplemented by Equation 27, $H(z)$ may be obtained. Jerk has the virtue that constant $j = 1$ corresponds to a cosmology that transitions from $a \propto t^{2/3}$ at early times to $a \propto e^{Ht}$ at late times. Moreover, for constant jerk, Equation 28 is easily solved:

$$\ln \left[\frac{q - q_+}{q - q_-} \right] = \exp \left[-2(q_+ - q_-)(1 + z) \right], \quad q_\pm = \frac{1}{4} \left(-1 \pm \sqrt{1 + 8j} \right). \qquad (29)$$

However, constant jerk does not span cosmology model space well: The asymptotic values of deceleration are $q = q_\pm$, so that there can only be a matter-dominated beginning ($q = \frac{1}{2}$) for $j = 1$. One would test for departures from ΛCDM by searching for variation of $j(z)$ from unity over some redshift interval; in principle, the same information is also encoded in $q(z)$.

The kinematic approach has produced some interesting results: Using the supernova data and the principal components method, Shapiro & Turner (2006) find the best-measured mode of $q(z)$ can be used to infer 5σ evidence for acceleration of the universe at some recent time, without recourse to GR and the Friedmann equation.

7. PROBES OF COSMIC ACCELERATION

As described in Section 4, the phenomenon of accelerated expansion is now well established, and the dark energy density has been determined to a precision of a few percent. However, getting at the nature of the dark energy—by measuring its equation-of-state parameter—is more challenging. To illustrate, consider that for fixed Ω_{DE}, a 1% change in (constant) w translates to only a 3% (0.3%) change in dark energy (total) density at redshift $z = 2$ and to only a 0.2% change in distances to redshifts $z = 1 - 2$.

The primary effect of dark energy is on the expansion rate of the universe; in turn, this affects the redshift-distance relation and the growth of structure. Although dark energy has been important during recent epochs, we expect that its effects at high redshift were very small, as otherwise it would have been difficult for large-scale structure (LSS) to have formed (in most models). Because $\rho_{DE}/\rho_M \propto (1 + z)^{3w} \sim 1/(1 + z)^3$, the redshifts of highest leverage for probing dark energy are expected to be between a few tenths and two (Huterer & Turner 2001). Four methods hold particular promise in probing dark energy in this redshift range: type Ia supernovae (SNe Ia), clusters of galaxies (CL), baryon acoustic oscillations (BAO), and weak gravitational lensing (WL). In this section, we describe and compare these four probes, highlighting their complementarity in terms of both dark energy constraints and the systematic errors to which they are susceptible. Because of this complementarity, a multipronged approach will be most effective. The goals of the next generation of dark energy experiments, described in Section 8, are to constrain w_0 at the few-percent level and w_a at the 10% level. Although we primarily focus on these four techniques, we also briefly discuss other dark energy probes, emphasizing the important supporting role of the CMB.

7.1. Supernovae

By providing bright, standardizable candles (Leibundgut 2001), SNe Ia constrain cosmic acceleration through the Hubble diagram, cf. Equation 11. The first direct evidence for cosmic acceleration came from SNe Ia, and they have provided the strongest constraints on the dark energy equation-of-state parameter. At present, they represent the most effective and mature probe of dark energy.

SNe Ia light curves are powered by the radioactive decays of ^{56}Ni (at early times) and ^{56}Co (after a few weeks), produced in the thermonuclear explosion of a carbon-oxygen white dwarf accreting mass from a companion star as it approaches the Chandrasekhar mass (Hillebrandt & Niemeyer 2000). The peak luminosity is determined by the mass of ^{56}Ni produced in the explosion (Arnett 1982): If the white dwarf is fully burned, one expects $\sim$0.6 $M_\odot$ of ^{56}Ni to be produced. As a result, although the detailed mechanism of SNe Ia explosions remains uncertain (e.g., Hoeflich 2004; Plewa, Calder & Lamb 2004), SNe Ia are expected to have similar peak luminosities. Because they are about as bright as a typical galaxy when they peak, SNe Ia can be observed to large distances, which highlights their utility as standard candles for cosmology.

In fact, as **Figure 12** shows, SNe Ia are not intrinsically standard candles, as they have a 1σ spread of order 0.3 mag in peak B band luminosity. However, work in the early 1990s (Phillips 1993) established an empirical correlation between SNe Ia peak brightness and the rate at which
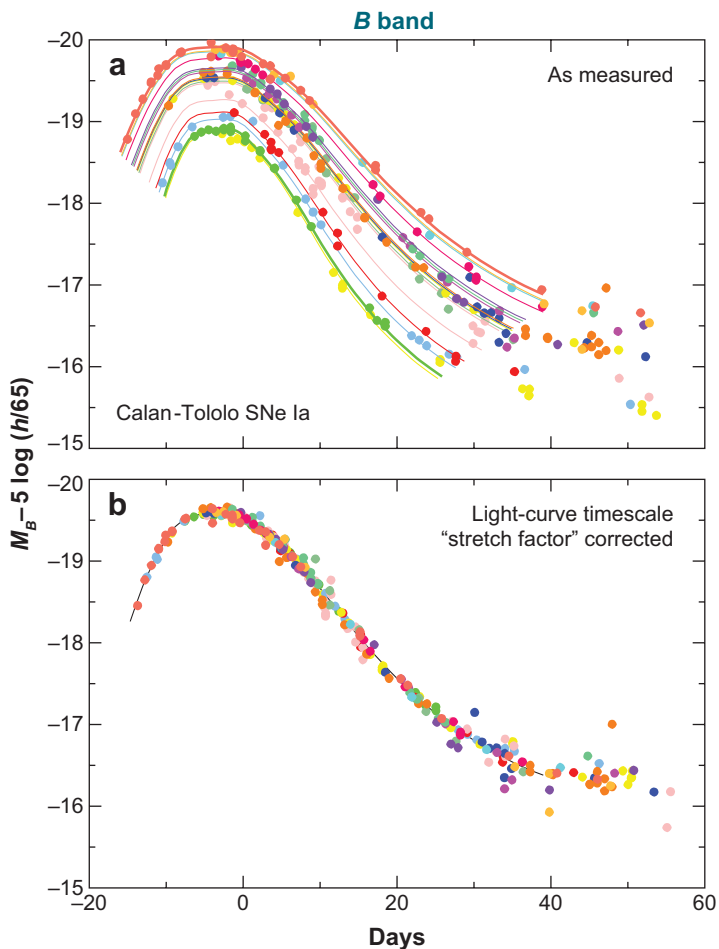
Figure 12

(*a*) B band light curves for low-redshift type Ia supernovae (SNe Ia) from the Calan-Tololo survey (Hamuy et al. 1996) show an intrinsic scatter of ∼0.3 mag in peak luminosity. (*b*) After a one-parameter correction for the brightness-decline correlation, the light curves show an intrinsic dispersion of only ∼0.15 mag. Figure reproduced from Kim (2004).

the luminosity declines with time after peak: Intrinsically brighter SNe Ia decline more slowly. After correcting for this correlation, SNe Ia turn out to be excellent standardizable candles, with a dispersion of about 15% in peak brightness.

Cosmological parameters are constrained by comparing distances to low- and high-redshift SNe Ia. Operationally, because $H_0 d_L$ is independent of the Hubble parameter H_0, Equation 11 can be written as $m = 5 \log_{10}[H_0 d_L(z; \Omega_M, \Omega_{DE}, w(z))] + \mathcal{M}$, where $\mathcal{M} \equiv M - 5 \log_{10}(H_0 \text{ Mpc}) + 25$ is the parameter effectively constrained by the low-redshift supernovae that anchor the Hubble diagram.

The major systematic concerns for supernova distance measurements are errors in correcting for host-galaxy extinction and uncertainty in the intrinsic colors of SNe Ia, luminosity evolution, and selection bias in the low-redshift sample. For observations in two passbands, with perfect knowledge of intrinsic supernova colors or of the extinction law, one could solve for the extinction

and eliminate its effects on the distance modulus. In practice, the combination of photometric errors, variations in intrinsic supernova colors, and uncertainties and likely variations in host-galaxy dust properties lead to distance uncertainties even for multiband observations of supernovae. Observations that extend into the rest-frame near infrared, where the effects of extinction are much reduced, offer promise in controlling this systematic.

With respect to luminosity evolution, there is evidence that supernova peak luminosity correlates with host-galaxy type (e.g., Jha, Riess & Kirshner 2007) and that the mean host-galaxy environment, e.g., the star formation rate, evolves strongly with look-back time. However, brightness-decline-corrected SNe Ia Hubble diagrams are consistent between different galaxy types, and because the nearby universe spans the range of galactic environments sampled by the high-redshift supernovae, one can measure distances to high-redshift events by comparing with low-redshift analogs. Although supernovae provide a number of correlated observables (e.g., multiband light curves and multiepoch spectra) to constrain the physical state of the system, insights from SNe Ia theory will likely be needed to determine if they are collectively sufficient to constrain the mean peak luminosity at the percent level (Hoeflich 2004).

Finally, there is concern that the low-redshift supernovae currently used to anchor the Hubble diagram and that serve as templates for fitting distant supernova light curves are a relatively small, heterogeneously selected sample and that correlated large-scale peculiar velocities induce larger distance errors than previously estimated (Hui & Greene 2006). This situation should improve in the near future once results are collected from low-redshift supernova surveys such as the Lick Observatory Supernova Search, the Center for Astrophysics Supernova project, the Carnegie Supernova Project, the Nearby Supernova Factory, and the SDSS-II Supernova Survey.

Accounting for systematic errors, precision measurement of w_0 and w_a with supernovae will require a few thousand SNe Ia light curves out to redshifts $z \sim 1.5$ to be measured with unprecedented precision and control of systematics (Frieman et al. 2003). For redshifts $z > 0.8$, this will require going to space to minimize photometric errors, to obtain uniform light curve coverage, and to observe in the near-infrared bands to capture the redshifted photons.

7.2. Galaxy Clusters

Clusters are the largest virialized objects in the universe. Within the context of the CDM paradigm, the number density of cluster-sized dark matter halos as a function of redshift and halo mass can be accurately predicted from N-body simulations (e.g., Warren et al. 2006). Comparing these predictions to large-area cluster surveys that extend to high redshift ($z \geq 1$) can provide precise constraints on the cosmic expansion history (Wang & Steinhardt 1998, Haiman, Mohr & Holder 2001).

The redshift distribution of clusters in a survey that selects clusters according to some observable O with redshift-dependent selection function $f(O, z)$ is given by

$$\frac{d^2 N(z)}{dz d\Omega} = \frac{r^2(z)}{H(z)} \int_0^\infty f(O, z) dO \int_0^\infty p(O|M, z) \frac{dn(z)}{dM} dM, \tag{30}$$

where $dn(z)/dM$ is the space density of dark halos in comoving coordinates and $p(O|M, z)$ is the mass-observable relation, the probability that a halo of mass M at redshift z is observed as a cluster with observable property O. The utility of this probe hinges on the ability to robustly associate cluster observables such as X-ray luminosity or temperature, cluster galaxy richness, Sunyaev-Zel'dovich effect (SZE) flux decrement, or weak lensing shear, with cluster mass (e.g., Borgani 2006).
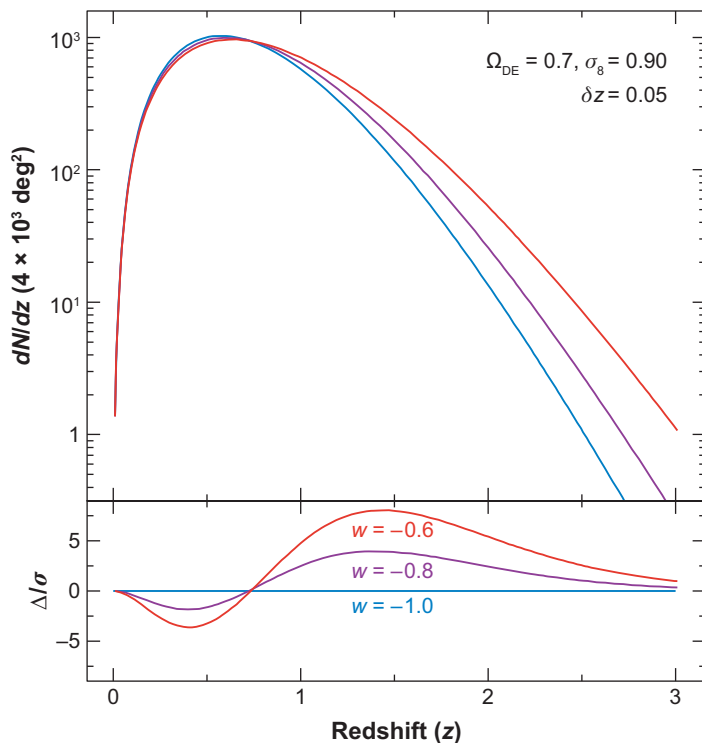
Figure 13

Predicted cluster counts for a survey covering 4000 deg², which is sensitive to halos more massive than
2×10^{14} $M_\odot$, for three flat cosmological models with fixed $\Omega_M = 0.3$ and $\sigma_8 = 0.9$. *Bottom*: Differences
between the models relative to the statistical errors. Reproduced from Mohr (2005).

The sensitivity of cluster counts to dark energy arises from two factors: geometry (the term
multiplying the integral in Equation 30 is the comoving volume element) and growth of struc-
ture [$dn(z)/dM$ depends on the evolution of density perturbations, cf. Equation 15]. The cluster
mass function is also determined by the primordial spectrum of density perturbations; its near-
exponential dependence upon mass is the root of the power of clusters to probe dark energy.

Figure 13 shows the sensitivity to the dark energy equation-of-state parameter of the expected
cluster counts for the South Pole Telescope and the Dark Energy Survey. At modest redshift,
$z < 0.6$, the differences are dominated by the volume element; at higher redshift, the counts are
more sensitive to the growth rate of perturbations.

The primary systematic concerns are uncertainties in the mass-observable relation $p(O|M, z)$
and in the selection function $f(O, z)$. The strongest cosmological constraints arise for those cluster
observables that are most strongly correlated with mass [i.e., for which $p(O|M, z)$ is narrow for fixed
M] and that have a well-determined selection function. There are several independent techniques
used both for detecting clusters and for estimating their masses using observable proxies. Future
surveys will aim to combine two or more of these techniques to cross-check cluster mass estimates
and thereby control systematic error. Measurements of the spatial correlations of clusters and
of the shape of the mass function provide additional internal calibration of the mass-observable
relation (Lima & Hu 2004, Majumdar & Mohr 2004).

With multiband CCD imaging, clusters can be efficiently detected as enhancements in the
surface density of early-type galaxies, and their observed colors provide photometric redshift

estimates that substantially reduce the projection effects that plagued early optical-cluster catalogs (Yee & Gladders 2002, Koester et al. 2007). Weak lensing and dynamical studies show that cluster richness correlates with cluster mass (Johnston et al. 2007) and can be used to statistically calibrate mass-observable relations. Most of the cluster baryons reside in hot, X-ray-emitting gas in approximate dynamical equilibrium in the dark matter potential well. Because X-ray luminosity is proportional to the square of the gas density, X-ray clusters are high-contrast objects for which the selection function is generally well determined. Empirically, X-ray luminosity and temperature are both found to correlate more tightly than optical richness with virial mass (Arnaud 2005, Stanek et al. 2006).

The hot gas in clusters also Compton scatters CMB photons as they pass through, leading to the Sunyaev-Zel'dovich effect (SZE) (Sunyaev & Zeldovich 1970), a measurable distortion of the blackbody CMB spectrum. It can be detected for clusters out to high redshift (e.g., Carlstrom, Holder & Reese 2002). Because the SZE flux decrement is linear in the gas density, it should be less sensitive than X-ray luminosity to gas dynamics (Motl et al. 2005, Nagai 2006). Finally, weak lensing can be used both to detect and to infer the masses of clusters. As lensing is sensitive to all mass along the line of sight, projection effects are a major concern for shear-selected cluster samples (White, van Waerbeke & Mackey 2002, Hennawi & Spergel 2005).

X-ray or SZE measurements also enable measurements of the baryonic gas mass in clusters; in combination with the virial mass estimates described above, this enables estimates of the baryon gas fraction, $f_{gas} \propto M_B/M_{tot}$. The ratio inferred from X-ray/SZE measurements depends upon cosmological distance because the inferred baryon mass, $M_B \propto d_L^{5/2}$ (X-ray) or $\propto d_L^2$ (SZE), and the inferred total mass from X-ray measurements $M_{tot} \propto d_L$. If clusters are representative samples of matter, then $f_{gas}(z) \propto d_L^{3/2 \text{ or } 1}$ should be independent of redshift and $\approx \Omega_B/\Omega_M$; this will only be true for the correct cosmology (Allen et al. 2007, Rapetti & Allen 2007).

7.3. Baryon Acoustic Oscillations

The peaks and troughs seen in the angular power spectrum of the CMB temperature anisotropy (see **Figure 5**) arise from gravity-driven acoustic oscillations of the coupled photon-baryon fluid in the early universe. The scale of these oscillations is set by the sound horizon at the epoch of recombination—the distance s over which sound waves in the fluid could have traveled by that time,

$$s = \int_0^{t_{rec}} c_s(1+z)\,dt = \int_{z_{rec}}^{\infty} \frac{c_s}{H(z)}\,dz, \tag{31}$$

where the sound speed c_s is determined by the ratio of the baryon and photon energy densities. The precise measurement of the angular scales of the acoustic peaks by WMAP has determined $s = 147 \pm 2$ Mpc. After recombination, the photons and baryons decouple and the effective sound speed of the baryons plummets due to the loss of photon pressure; the sound waves remain imprinted in the baryon distribution and, through gravitational interactions, in the dark matter distribution as well. Because the sound horizon scale provides a standard ruler calibrated by the CMB anisotropy, measurement of the BAO scale in the galaxy distribution provides a geometric probe of the expansion history.

In the galaxy power spectrum, this scale appears as a series of oscillations with amplitude of order 10%, which is more subtle than the acoustic oscillations in the CMB because the impact of baryons on the far larger dark matter component is small. Measuring the BAO scale from galaxy clustering in the transverse and line-of-sight directions yields measurements of $r(z)/s$ and of $s\,H(z)$, respectively (Blake & Glazebrook 2003, Hu & Haiman 2003, Seo & Eisenstein 2003).

Spectroscopic redshift surveys can probe both, whereas photometric surveys are sensitive mainly to transverse clustering. Although determining these quantities with precision requires enormous survey volumes and millions of galaxies, N-body simulations suggest that the systematic uncertainties associated with BAO distance-scale measurements are smaller than those of other observational probes of dark energy. Because such large numbers of galaxies are needed, BAO measurements provide distance estimates that are coarse grained in redshift.

The main systematic uncertainties in the interpretation of BAO measurements are the effects of nonlinear gravitational evolution, scale-dependent differences between the clustering of galaxies and of dark matter (bias), and for spectroscopic surveys, redshift distortions of the clustering, which can shift the BAO features. Numerical studies performed to date suggest that the resulting shift of the scale of the BAO peak in the galaxy power spectrum is at the percent level or less (Guzik, Bernstein & Smith 2007; Seo & Eisenstein 2007; Smith, Scoccimarro & Sheth 2007), comparable to the forecast measurement uncertainty for future surveys but in principle predictable from high-resolution simulations.

7.4. Weak Gravitational Lensing

The gravitational bending of light by structures in the universe distorts or shears the images of distant galaxies (**Figure 14**). This distortion allows the distribution of dark matter and its evolution with time to be measured, thereby probing the influence of dark energy on the growth of structure.

The statistical signal due to gravitational lensing by LSS is termed cosmic shear. The cosmic shear field at a point in the sky is estimated by locally averaging the shapes of large numbers of distant galaxies. The primary statistical measure of the cosmic shear is the shear angular power spectrum, which is measured as a function of source-galaxy redshift z_s. (Additional information is obtained by measuring the correlations between shears at different redshifts or with foreground
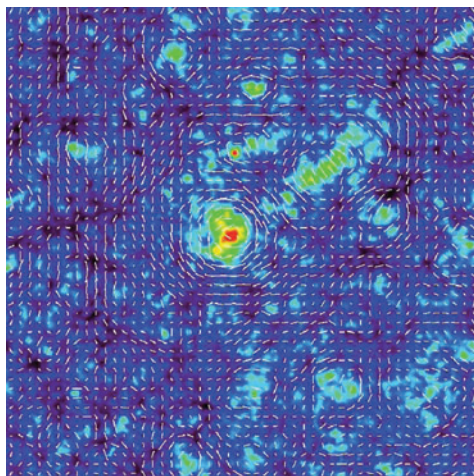

Figure 14

Cosmic shear field (*white ticks*) superimposed on the projected mass distribution from a cosmological N-body simulation. Overdense regions appear bright; underdense regions appear dark. Note that the shear field is correlated with the foreground mass distribution. Figure used with permission from T. Hamana.

lensing galaxies.) The shear angular power spectrum is (Kaiser 1992, Hu & Jain 2004)

$$P_\ell^\gamma(z_s) = \int_0^{z_s} dz \frac{H(z)}{d_A^2(z)} |W(z, z_s)|^2 P_\rho\left(k = \frac{\ell}{d_A(z)}; z\right),$$ (32)

where ℓ is the angular multipole, the weight function $W(z, z_s)$ is the efficiency for lensing a population of source galaxies and is determined by the distance distributions of the source and lens galaxies, and $P_\rho(k, z)$ is the power spectrum of density perturbations.

As with clusters, the dark energy sensitivity of the shear angular power spectrum comes from two factors: geometry (the Hubble parameter, the angular-diameter distance, and the weight functions) and growth of structure (through the evolution of the power spectrum of density perturbations). It is also possible to separate these effects and extract a purely geometric probe of dark energy from the redshift dependence of galaxy-shear correlations (Jain & Taylor 2003, Bernstein & Jain 2004). The three-point correlation of cosmic shear is also sensitive to dark energy (Takada & Jain 2004).

The statistical uncertainty in measuring the shear power spectrum on large scales is (Kaiser 1992)

$$\Delta P_\ell^\gamma = \sqrt{\frac{2}{(2\ell+1)f_{\text{sky}}}} \left[P_\ell^\gamma + \frac{\sigma^2(\gamma_i)}{n_{\text{eff}}}\right],$$ (33)

where f_{sky} is the fraction of sky area covered by the survey, $\sigma^2(\gamma_i)$ is the variance in a single component of the (two-component) shear, and n_{eff} is the effective number density per steradian of galaxies with well-measured shapes. The first term in brackets, which dominates on large scales, comes from cosmic variance of the mass distribution, and the second, shot-noise term results both from the variance in galaxy ellipticities (known as shape noise) and from shape-measurement errors due to noise in the images. **Figure 15** shows the shear power spectrum's dependence on dark energy and an indication of the statistical errors expected for a project such as the Large Synoptic
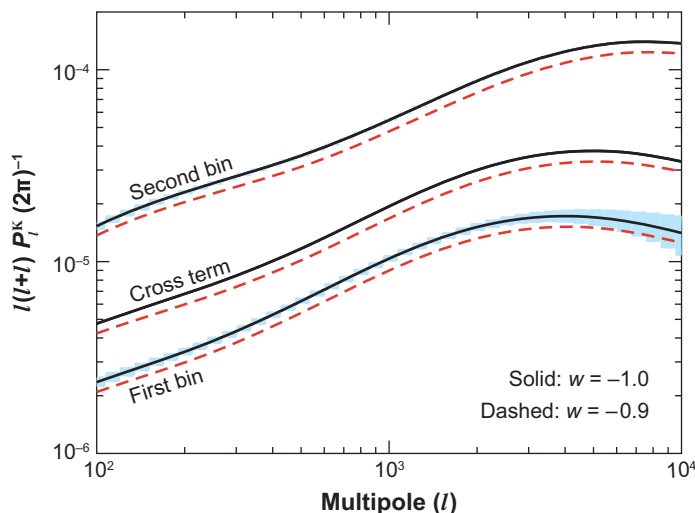

Figure 15

Cosmic shear angular power spectrum and statistical errors expected for the Large Synoptic Survey Telescope for $w = -1$ and $w = -0.9$. For illustration, results are shown for source galaxies in two broad redshift bins, $z_s = 0 - 1$ (*first bin*) and $z_s = 1 - 3$ (*second bin*). The cross-power spectrum between the two bins (*cross term*) is shown without the statistical errors.

Survey Telescope (LSST), assuming a survey area of 15,000 deg^2 and an effective source-galaxy density of $n_{eff} = 30$ galaxies per arcmin^2.

Systematic errors in weak lensing measurements arise from a number of sources (Huterer et al. 2006), including incorrect shear estimates, uncertainties in galaxy photometric redshift estimates, intrinsic correlations of galaxy shapes, and theoretical uncertainties in the mass power spectrum on small scales. The dominant cause of galaxy-shape measurement error in current lensing surveys is the anisotropy of the image point spread function caused by optical and CCD distortions, tracking errors, wind shake, atmospheric refraction, etc. This error can be diagnosed because there are geometric constraints on the shear patterns that can be produced by lensing that are not respected by systematic effects. A second kind of shear measurement error arises from miscalibration of the relation between measured galaxy shape and inferred shear, which results from inaccurate correction for the circular blurring of galaxy images due to atmospheric seeing. Photometric redshift errors impact shear power spectrum estimates primarily through uncertainties in the scatter and bias of photometric redshift estimates in redshift bins (Huterer et al. 2006; Ma, Hu & Huterer 2006). Any tendency of galaxies to align with their neighbors—or to align with the local mass distribution—can be confused with alignment caused by gravitational lensing, thus biasing dark energy determinations (Hirata & Seljak 2004, Heymans et al. 2006). Finally, uncertainties in the theoretical mass power spectrum on small scales could complicate attempts to use the high-multipole ($\ell \geq$ several hundred) shear power spectrum to constrain dark energy. Fortunately, weak lensing surveys should be able to internally constrain the impact of such effects (Zentner, Rudd & Hu 2007).

7.5. Other Probes

Although the four methods discussed above have the most probative power, a number of other methods have been proposed, offering the possibility of additional consistency checks. The Alcock-Paczynski test exploits the fact that the apparent shapes of intrinsically spherical cosmic structures depend on cosmology (Alcock & Paczynski 1979). Because spatial clustering is statistically isotropic, the anisotropy of the two-point correlation function along and transverse to the line of sight has been proposed for this test, e.g., using the Lyman alpha forest (Hui, Stebbins & Burles 1999).

Weak lensing of the CMB anisotropy by foreground clusters, in combination with lensing of galaxies, provides a potential geometric probe of dark energy (e.g., Hu, Holz & Vale 2007). The ISW effect provides a confirmation of cosmic acceleration, cf. Section 4.1.2. ISW impacts the large-angle structure of the CMB anisotropy, but low-ℓ multipoles are subject to large cosmic variance, limiting their power. Nevertheless, ISW is of interest because it may be able to show the imprint of large-scale dark energy perturbations (Coble, Dodelson & Frieman 1997; Hu & Scranton 2004).

Gravitational radiation from inspiraling binary neutron stars or black holes can serve as standard sirens to measure absolute distances. If their redshifts can be determined, then they could be used to probe dark energy through the Hubble diagram (Dalal et al. 2006).

Long-duration gamma-ray bursts have been proposed as standardizable candles (e.g., Schaefer 2003), but their utility as cosmological distance indicators that could be competitive with or complementary to SNe Ia has yet to be established (Friedman & Bloom 2005). The angular size-redshift relation for double radio galaxies has also been used to derive cosmological constraints that are consistent with dark energy (Guerra, Daly & Wan 2000). The optical depth for strong gravitational lensing (multiple imaging) of quasi-stellar objects (QSOs) or radio sources has been proposed (Fukugita et al. 1992) and used (e.g., Mitchell et al. 2005, Chae 2007) to provide

independent evidence for dark energy, although these measurements depend on modeling the density profiles of lens galaxies.

In principle, polarization measurements from distant clusters provide a sensitive probe of the growth function and hence dark energy (Cooray, Huterer & Baumann 2004). The relative ages of galaxies at different redshifts, if they can be determined reliably, provide a measurement of dz/dt and, from Equation 13, measure the expansion history directly (Jimenez & Loeb 2002). Measurements of the abundance of lensed arcs in clusters, if calibrated accurately, provide a probe of dark energy (Meneghetti et al. 2005).

As we have stressed, there is every reason to expect that at early times dark energy was but a tiny fraction of the energy density. Big bang nucleosynthesis and CMB anisotropy have been used to test this prejudice, and current data already indicate that dark energy at early times contributes no more than ~5% of the total energy density (Bean, Hansen & Melchiorri 2001; Doran & Robbers 2006).

7.6. Role of the Cosmic Microwave Background

Although the CMB provides precise cosmological constraints, by itself it has little power to probe dark energy. The reason is simple: The CMB provides a single snapshot of the universe at a time when dark energy contributed but a tiny part of the total energy density (a part in 10^9 for vacuum energy). Nonetheless, the CMB plays a critical supporting role by determining other cosmological parameters, such as the spatial curvature and matter density, to high precision, thereby considerably strengthening the power of the methods discussed above (cf. **Figure 8**). It also provides the standard ruler for BAO measurements. Data from the Planck CMB mission, scheduled for launch in 2008, will complement those from dark energy surveys. If the Hubble parameter can be directly measured to better than a few percent, in combination with Planck it would also provide powerful dark energy constraints (Hu 2005).

7.7. Probing New Gravitational Physics

In Section 5.2 we discussed the possibility that cosmic acceleration could be explained by a modification of GR on large scales. How can we distinguish this possibility from dark energy within GR and/or test the consistency of GR to explain cosmic acceleration? Because modified gravity can change both the Friedmann equations and the evolution of density perturbations, a strategy for testing the consistency of GR and dark energy as the explanation for acceleration is to compare results from the geometric (expansion history) probes, e.g., supernovae or BAO, with those from the probes sensitive to the growth of structure, e.g., clusters or weak lensing. Differences between the two could be evidence for the need to modify GR (Knox, Song & Tyson 2006). A first application of this idea to current data shows that standard GR passes a few modest consistency tests (Chu & Knox 2005, Wang et al. 2007). Finally, any modification of gravity may have observable effects beyond cosmology, and precision solar system tests can provide important additional constraints (e.g., Lue, Scoccimarro & Starkman 2004).

7.8. Summary and Comparison

Four complementary cosmological techniques, WL, SNe Ia, BAO, and CL, have the power to probe dark energy with high precision and thereby advance our understanding of cosmic acceleration. To date, constraints upon the dark energy equation-of-state parameter have come from combining the results of two or more techniques, e.g., SN + BAO + CMB (see **Figure 8**) or

Table 2 Comparison of dark energy probes

Method	Strengths	Weaknesses	Systematics
WL	Growth + geometric, statistical power	CDM assumption	Image quality, photo-z
SNe	Purely geometric, mature	Standard candle assumption	Evolution, dust
BAO	Largely geometric, low systematics	Large samples required	Bias, nonlinearity
CL	Growth + geometric, X-ray + SZ + optical	CDM assumption	Determining mass, selection function

Abbreviations: BAO, baryon acoustic oscillations; CDM, cold dark matter; CL, galaxy clusters; SNe, supernovae; WL, weak gravitational lensing.

BAO + CMB (see **Table 1**), in order to break cosmological parameter degeneracies. In the future, each of these methods, in combination with CMB information that constrains other cosmological parameters, will provide powerful individual constraints on dark energy; collectively, they should be able to approach percent-level precision on w at its best-constrained redshift, i.e., w_p (see **Figure 17**).

Table 2 summarizes the strengths and weaknesses and the primary systematic errors of these four dark energy probes. **Figure 16** gives a visual impression of the statistical power of each of these techniques in constraining dark energy, showing how much each of them could be expected to improve our present knowledge of w_0 and w_a in a dedicated space mission (Albrecht et al. 2006).

8. DARK ENERGY PROJECTS

A diverse and ambitious set of projects to probe dark energy is in progress or in the planning stages. Here we provide a brief overview of the observational landscape. With the exception of experiments at the LHC that may shed light on dark energy through discoveries about SUSY or dark matter, all planned experiments involve cosmological observations. **Table 3** provides a representative sample, not a comprehensive list, of projects that have been proposed or are currently under construction. It does not include experiments that have already reported results.
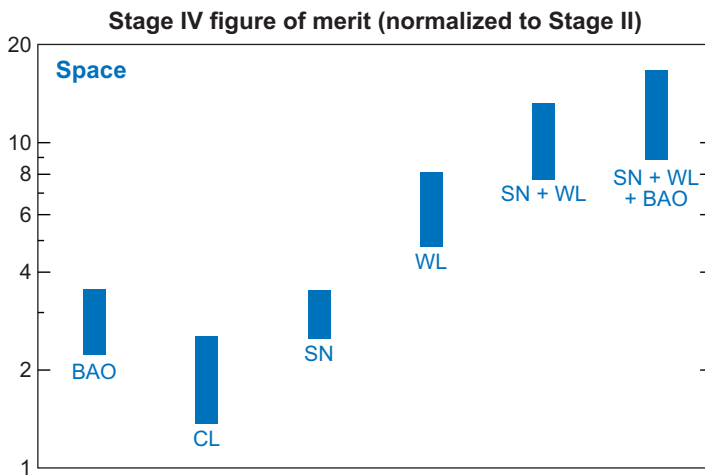

Figure 16

Relative statistical power of different dark energy space probes, separately and in combination, in constraining the Dark Energy Task Force figure of merit. The blue bars indicate the estimated range of increase (allowing for uncertainties in systematic errors) in the figure of merit relative to present experiments. Adopted from the Dark Energy Task Force report (Albrecht et al. 2006).

Table 3 Dark energy projects proposed or under construction

Survey	Description	Probes	Stage[a]
Ground-based:			
ACT	SZE, 6-m	CL	II
APEX	SZE, 12-m	CL	II
SPT	SZE, 10-m	CL	II
VST	Optical imaging, 2.6-m	BAO, CL, WL	II
Pan-STARRS 1(4)	Optical imaging, 1.8-m($\times$4)	All	II(III)
DES	Optical imaging, 4-m	All	III
Hyper Suprime-Cam	Optical imaging, 8-m	WL, CL, BAO	III
ALPACA	Optical imaging, 8-m	SN, BAO, CL	III
LSST	Optical imaging, 6.8-m	All	IV
AAT WiggleZ	Spectroscopy, 4-m	BAO	II
HETDEX	Spectroscopy, 9.2-m	BAO	III
PAU	Multifilter imaging, 2-3-m	BAO	III
SDSS BOSS	Spectroscopy, 2.5-m	BAO	III
WFMOS	Spectroscopy, 8-m	BAO	III
HSHS	21-cm radio telescope	BAO	III
SKA	km^2 radio telescope	BAO, WL	IV
Space-based:			
JDEM Candidates			
ADEPT	Spectroscopy	BAO, SN	IV
DESTINY	Grism spectrophotometry	SN	IV
SNAP	Optical+NIR+spectro	All	IV
Proposed ESA Missions			
DUNE	Optical imaging	WL, BAO, CL	
SPACE	Spectroscopy	BAO	
eROSITA	X-ray	CL	
CMB Space Probe			
Planck	SZE	CL	
Beyond Einstein Probe			
Constellation-X	X-ray	CL	IV

[a]Stage refers to the Dark Energy Task Force timescale classification.

Abbreviations: BAO, baryon acoustic oscillations; CL, galaxy clusters; CMB, cosmic microwave background; ESA, European Space Agency; JDEM, Joint Dark Energy Mission; NIR, near-infrared; SN, supernova; SZE, Sunyaev-Zel'dovich effect; WL, weak gravitational lensing.

Surveys: ACT, Atacama Cosmology Telescope; ADEPT, Advanced Dark Energy Physics Telescope; ALPACA, Advanced Liquid-Mirror Probe of Asteroids, Cosmology, and Astrophysics; APEX, Atacama Pathfinder Experiment; DES, Dark Energy Survey; DESTINY, Dark Energy Space Telescope; DUNE, Dark Universe Explorer; eROSITA, extended Roentgen Survey with an Imaging Telescope Array; HETDEX, Hobby Eberly Telescope Dark Energy Experiment; HSHS, Hubble Sphere Hydrogen Survey; LSST, Large Synoptic Survey Telescope; Pan-STARRS, Panoramic Survey Telescope and Rapid Response System; PAU, Physics of the Accelerating Universe; SDSS BOSS, Sloan Digital Sky Survey/Baryon Oscillation Sky Survey; SKA, Square Kilometer Array; SNAP, Supernova Acceleration Probe; SPACE, Spectroscopic All-sky Cosmic Explorer; SPT, South Pole Telescope; VST, VLT Survey Telescope; WFMOS, Wide-Field Multi-Object Spectrograph.

All of these projects share the common feature of surveying wide areas to collect large samples of objects—galaxies, clusters, or supernovae.

The Dark Energy Task Force (DETF) report (Albrecht et al. 2006) classified dark energy surveys into an approximate sequence: Ongoing projects, either taking data or soon to be taking data, are Stage II; near-future, intermediate-scale projects are Stage III; and larger-scale, longer-term future projects are Stage IV. More advanced stages are in general expected to deliver tighter dark energy constraints, which the DETF quantified using the w_0-w_a figure of merit (FoM) discussed in the Appendix. Stage III experiments are expected to deliver a factor $\sim 3 - 5$ improvement in the DETF FoM compared to the combined Stage II results, whereas Stage IV experiments should improve the FoM by roughly a factor of 10 compared to Stage II. However, these estimates are only indicative and are subject to considerable uncertainties in systematic errors (see **Figure 16**).

We divide our discussion in Sections 8.1 and 8.2 into ground- and space-based surveys. Ground-based projects are typically less expensive than their space-based counterparts and can employ larger-aperture telescopes. The discovery of dark energy and many of the subsequent observations to date have been dominated by ground-based telescopes. However, high-redshift SN observations, Chandra (X-ray clusters), and WMAP CMB observations have played critical roles in probing dark energy. Although they are more challenging to execute, space-based surveys offer the advantages of observations unhindered by weather and by the scattering, absorption, and emission by the atmosphere, stable observing platforms free of time-changing gravitational loading, and the ability to continuously observe away from the sun and moon. They therefore have the potential for greatly improving control of systematic errors.

8.1. Ground-Based Surveys

A number of projects to detect clusters and probe dark energy using the SZE (see Section 7.2) are under way. These surveys are coordinated with optical surveys that can determine cluster redshifts. The Atacama Pathfinder Experiment (APEX) survey in Chile will cover up to 1000 deg^2. The largest of these projects are the Atacama Cosmology Telescope (ACT) and the South Pole Telescope (SPT); the latter will carry out a 4000-deg^2 survey.

A number of planned or proposed optical imaging surveys can study dark energy through weak lensing, clusters, and angular BAO using a single wide-area survey. These projects use telescopes of intermediate to large aperture and wide field-of-view along with gigapixel-scale CCD cameras, and they are deployed at the best astronomical sites in order to obtain deep-galaxy photometry and shape measurements. They deliver photometric-redshift information through color measurements using multiple passbands. The European Southern Observatory's (ESO's) VLT Survey Telescope (VST) on Cerro Paranal will carry out public surveys, including the 1500-deg^2 Kilo-Degree Survey (KIDS) and a shallower, 4,500-deg^2 survey (known as ATLAS). The Panoramic Survey Telescope and Rapid Response System (Pan-STARRS)-1 uses a 1.8-m wide-field telescope to carry out several wide-area surveys from Haleakala; in the future, 4×1.8-m telescopes may be deployed at Mauna Kea in Pan-STARRS-4. The Dark Energy Survey (DES) will use a new 3-deg^2 imager with red-sensitive CCDs on a 4-m telescope at Cerro Tololo Inter-American Observatory (CTIO) in Chile to carry out a 5000-deg^2 survey in five optical passbands, covering the same survey area as the SPT and partnering with the ESO Visible and Infrared Survey Telescope for Astronomy (VISTA) Hemisphere Survey, which will survey the same area in three near-infrared bands. Hyper Suprime-Cam is a new wide-field imager planned for the Subaru telescope on Mauna Kea and will be used to carry out a deep survey over 2000 deg^2. The Advanced Liquid-Mirror Probe of Asteroids, Cosmology, and Astrophysics (ALPACA) is a proposed rotating liquid-mercury telescope that would repeatedly survey a long, narrow strip of the sky at CTIO. The most ambitious of these

projects is the LSST, which would deploy a multigigapixel camera with a 10-deg^2 field of view on a new telescope on Cerro Pachon in Chile to survey 15,000 deg^2 over 10 years.

Several large spectroscopic surveys have been designed to detect BAO by measuring $\sim 10^5 - 10^9$ galaxy and QSO redshifts using large multifiber spectrographs. WiggleZ is using the Anglo-Australian Telescope to collect spectra of 400,000 galaxies in the redshift range $0.5 < z < 1$. The Baryon Oscillation Sky Survey (BOSS) plans to use the SDSS telescope in New Mexico to measure 1.5 million galaxy spectra out to $z = 0.7$. The Hobby Eberly Telescope Dark Energy Experiment (HETDEX) plans to target Lyman alpha emitters at higher redshift, $2 \leq z \leq 4$. The Wide-Field Multi-Object Spectrograph (WFMOS), proposed for the Subaru telescope, would target galaxies at $z \leq 1.3$ and Lyman-break galaxies at $2.5 \leq z \leq 3.5$. The Physics of the Accelerating Universe (PAU) is a Spanish project to deploy a wide-field camera with a large number of narrow filters to measure coarse-grained galaxy spectra out to $z = 0.9$.

Finally, the proposed Square Kilometer Array (SKA), an array of radio antennas with unprecedented collecting area, would probe dark energy using BAO and WL of galaxies via measurements of the 21-cm line signature of neutral hydrogen. The Hubble Sphere Hydrogen Survey (HSHS) aims to carry out a 21-cm BAO survey on a shorter timescale.

8.2. Space-Based Surveys

Three of the proposed space projects are candidates for the Joint Dark Energy Mission (JDEM), a joint mission of the U.S. Department of Energy and the National Aeronautics and Space Administration's (NASA's) Beyond Einstein program, targeted at dark energy science. Supernova/Acceleration Probe (SNAP) proposes to study dark energy using a dedicated 2-m class telescope. With imaging in nine optical and near-infrared passbands and follow-up spectroscopy of supernovae, SNAP is designed principally to probe SNe Ia and WL, taking advantage of the excellent optical image quality and near-infrared transparency of a space-based platform. **Figure 17**
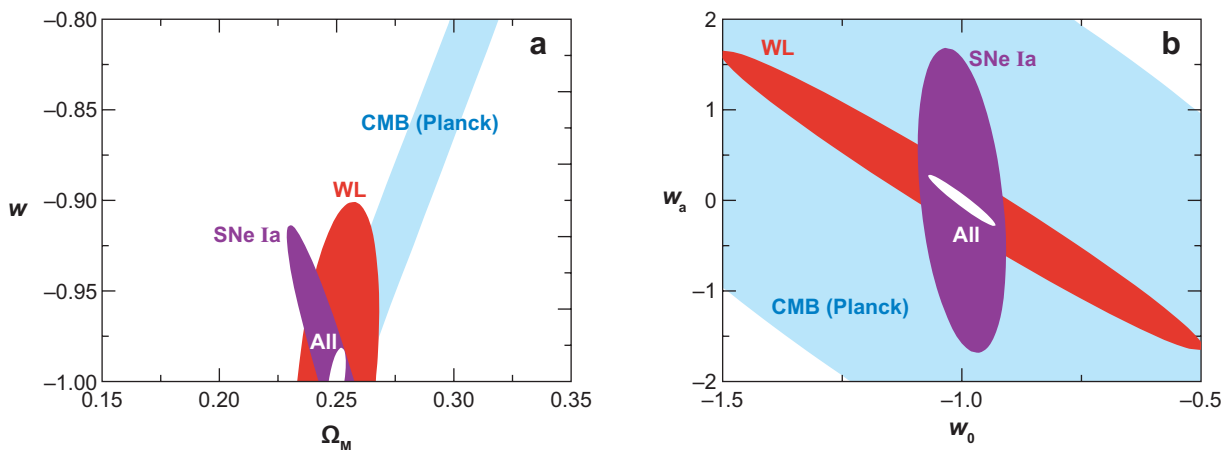

Figure 17

Illustration of forecast constraints on dark energy parameters. Shown are 68%-CL uncertainties for one version of the proposed Supernova/Acceleration Probe experiment, which combines a narrow-area survey of 2000 type Ia supernovae (SNe Ia) to $z = 1.7$ and a weak lensing (WL) survey of 1000 deg^2. (*a*) Constraints in the Ω_M-w plane, assuming constant w; the vertical axis can also be interpreted as the pivot value w_p for a time-varying equation of state. (*b*) Constraints in the w_0-w_a plane for time-varying dark energy equation of state, marginalized over Ω_M, for a flat universe.

illustrates the statistical constraints that the proposed SNAP mission could achieve by combining SNe Ia and WL observations with results from the Planck CMB mission. This forecast makes use of the Fisher information matrix described in the Appendix.

The Dark Energy Space Telescope (DESTINY) would use a similar-size telescope with a near-infrared grism spectrograph to study supernovae. The Advanced Dark Energy Physics Telescope (ADEPT) is a spectroscopic mission with the primary goal of constraining dark energy via BAO at $z \sim 2$ as well as supernovae. Another proposed mission within NASA's Beyond Einstein program is Constellation-X, which could observe X-ray clusters with unprecedented sensitivity.

There is one European Space Agency (ESA) mission nearing launch and two concepts under study. The Planck mission, planned for launch in late 2008, in addition to pinning down other cosmological parameters important for dark energy, will detect thousands of clusters using the SZE. Dark Universe Explorer (DUNE) and SPACE are optical missions to study dark energy using WL and BAO, respectively. They were each proposed for ESA's Cosmic Visions program and have recently been merged into a joint mission concept called Euclid. Finally, the extended Roentgen Survey with an Imaging Telescope Array (eROSITA), a German-Russian collaboration, is a planned X-ray telescope that will study dark energy using the abundance of X-ray clusters.

9. DARK ENERGY AND COSMIC DESTINY

One of the first things one learns in cosmology is that geometry is destiny: A closed (positively curved) universe eventually recollapses, and an open (flat or negatively curved) universe expands forever. Provided that the universe contains only matter and $\Lambda = 0$, this statement follows directly from Equation 2. The presence of dark energy severs this well-known connection between geometry and destiny and raises fundamental issues involving the distant future of our universe (Krauss & Turner 1995).

To illustrate the geometry-destiny connection, we can rewrite Equation 2 in terms of an effective potential and a kinetic energy term,

$$V_{\text{eff}}(a) + \dot{a}^2 = 0 \qquad V_{\text{eff}}(a) = k - \Omega_0 H_0^2 a^{-(1+3w_{\text{T}})}, \qquad (34)$$

where w_{T} is the ratio of the total pressure to the total energy density (including all components). If $w_{\text{T}} > -\frac{1}{3}$, as would be the case with only matter and radiation, then the second term in V_{eff} increases monotonically from $-\infty$ to 0 as a goes from 0 to ∞, which means that V_{eff} rises from $-\infty$ to k. For $k > 0$, there is a value of a where $V_{\text{eff}} \rightarrow 0$, at which point $\dot{a}$ must go to zero and where a achieves its maximum value. For $k = 0$, $\dot{a}$ only vanishes for $a \rightarrow \infty$, and for $k < 0$, $\dot{a}$ remains positive even as $a \rightarrow \infty$.

With dark energy there is a new twist: Because the dark energy density decreases more slowly than that of matter or radiation, as the universe expands dark energy eventually dominates the second term in V_{eff}. Thereafter, V_{eff} decreases monotonically, as $w_{\text{T}} \simeq w_{\text{DE}} < -\frac{1}{3}$, approaching $-\infty$ as $a \rightarrow \infty$. Provided that $\rho_{\text{DE}} > 0$ and that w_{DE} remains negative, if the scale factor becomes large enough for dark energy to dominate—which happens unless $\Omega_{\text{M}} > 1 \gg \Omega_{\text{DE}}$—then the universe will expand forever, irrespective of k.

If dark energy is vacuum energy, acceleration will continue, and the expansion will become exponential, leading to a "red out" of the universe. To better understand this, consider the comoving distance to fixed redshift z at time t during the epoch of exponential expansion:

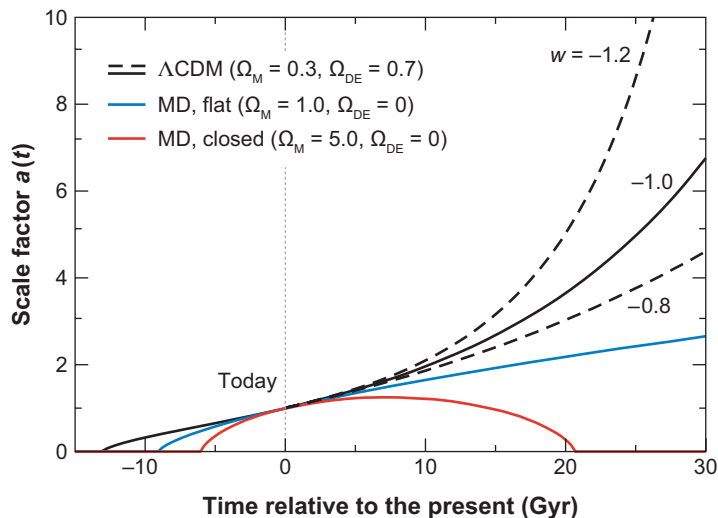$$r(z, t) = \int_{a(t)/(1+z)}^{a(t)} \frac{da}{a^2 H} \simeq z H_0^{-1} \exp[-H_0(t - t_0)]. \qquad (35)$$

Figure 18

Evolution of the Friedmann-Robertson-Walker scale factor in models with and without dark energy. The upper four curves are for flat models. The dashed curves denote models with $w = -0.8$ or -1.2 and $\Omega_M = 0.3$. Abbreviations: CDM, cold dark matter; MD, matter-dominated models.

The exponential decrease of this distance implies that the number of galaxies below a fixed redshift shrinks exponentially. By contrast, in the Einstein–de Sitter model with $\Omega_M = 1$, this distance increases as $t^{1/3}$ so that the number of galaxies with redshift less than a fixed value grows slowly. Alternatively, Equation 35 implies that the redshift for a galaxy at current distance r grows exponentially. Galaxies beyond the Local Group, $r \geq 1-2$ Mpc, will be redshifted beyond detectability on a timescale of $t - t_0 \sim 100$ Gyr (e.g., Busha et al. 2003). The Milky Way will remain gravitationally bound to the Local Group, which will appear as a static, "island" universe (Nagamine & Loeb 2003). Even the CMB, the other key evidence of a once-hot, expanding universe, will be redshifted to undetectability (Krauss & Scherrer 2007).

If dark energy is a scalar field, then eventually the field relaxes to the minimum of its potential (see **Figure 10**). If the minimum of the potential energy is precisely zero, the universe will again become matter dominated and will return to decelerated expansion, restoring the link between geometry and destiny. If the minimum of the scalar-field potential has negative energy density, the energy of dark matter and of scalar-field energy will eventually cancel, leading to recollapse, irrespective of k. If the potential energy at the minimum is positive and is larger than a critical value that depends on Ω_M (the critical value is zero for $\Omega_M \leq 1$ and small for $\Omega_M > 1$), then accelerated expansion will eventually ensue again and, as discussed above, the universe will experience a red-out. These possibilities are illustrated in **Figure 18**.

Finally, the possibility of $w_{DE} < -1$ deserves special mention. In this case, the energy density of dark energy actually increases with time, $\rho_{DE} \propto a^\beta$, where $\beta \equiv -3(1 + w) > 0$. In turn, the scale factor grows very rapidly and reaches infinite size in a finite time:

$$a(t) \simeq \frac{1}{[1 - \beta H_0(t - t_0)/2]^{2/\beta}}, \quad (t_\infty - t_0) \simeq \frac{2}{\beta H_0}. \quad (36)$$

This is the big rip scenario studied by Caldwell, Kamionkowski & Weinberg (2003). Once the density of dark energy exceeds that of any structure—from clusters to atoms—that structure is torn apart.

The presence of dark energy severs the simple relation between geometry and destiny, links destiny to an understanding of dark energy, raises the specter of a bleak future for cosmologists, and raises a deep question (Krauss & Turner 1995): Can we ever determine the future of the universe with certainty? As a thought experiment, ignore the current epoch of accelerated expansion and imagine instead that the universe has been determined to be matter dominated and that it is flat. We might be tempted to conclude that the universe will expand forever at an ever-decreasing rate. However, no matter how precise our measurements are, there could be a small cosmological constant lurking below the threshold of detectability. For example, if the vacuum energy density were one-billionth of the present matter density, after a factor of 1000 in expansion vacuum energy would come to dominate. If it were positive, exponential expansion would eventually ensue; if negative, the universe would ultimately recollapse. Only a fundamental understanding of the constituents of the universe and their relative abundances could deliver certainty about the destiny of the universe.

10. CONCLUDING REMARKS

Ten years after its discovery, the acceleration of the expansion of the universe is now firmly established. The physical origin of this phenomenon, however, remains a deep mystery, linked to other important problems in physics and astronomy. At present, the simplest explanation, vacuum energy, is consistent with all extant data, but theory provides no understanding of why it should have the requisite small value. Probing the history of cosmic expansion with much greater precision (few percent versus current 10%) offers the best hope of guiding us to a solution. An impressive array of experiments with that aim are being planned or are under way, and we believe that significant progress will be made within the next 15 years.

We conclude with our list of 10 important take-home facts about cosmic acceleration and dark energy, followed by our views on key open issues and challenges for the future.

10.1. Take-Home Facts

10.1.1. Strong evidence for accelerated expansion. Since the supernova discovery of acceleration, several hundred supernovae have been observed over a broader range of redshifts, substantially strengthening the case both statistically and by reducing sources of systematic error. Further, independent of GR and based solely upon the supernova Hubble diagram, there is very strong (5σ) evidence that the expansion of the universe accelerated recently (Shapiro & Turner 2006).

10.1.2. Dark energy as the cause of cosmic acceleration. Within GR, accelerated expansion cannot be explained by any known form of matter or energy, but it can be accommodated by a nearly smooth form of energy with large negative pressure, known as dark energy, that accounts for about 75% of the universe.

10.1.3. Independent evidence for dark energy. In the context of the CDM model of structure formation, CMB and LSS data provide independent evidence that the universe contains a smooth form of energy that accounts for about 75% of the total and that only came to dominate after essentially all of the observed structure had formed. Thus, structure formation independently points to a negative pressure (with $w \le -\frac{1}{3}$) dark energy accounting for the bulk of the universe.

10.1.4. Vacuum energy as dark energy. The simplest explanation for dark energy is the energy associated with the vacuum; it is mathematically equivalent to a cosmological constant. However,

all attempts to compute the vacuum energy density from the zero-point energies of all quantum fields yield a result that is many orders of magnitude too large or infinite.

10.1.5. Current observational status. Taken together, all the current data provide strong evidence for the existence of dark energy; they constrain the fraction of critical density contributed by dark energy, 0.76 ± 0.02, and the equation-of-state parameter, $w \approx -1 \pm 0.1$ (stat) ± 0.1 (sys), assuming that w is constant. These data imply that the universe began accelerating at redshift $z \sim 0.4$ and age $t \sim 10$ Gyr. These results are robust—data from any one method can be removed without compromising the constraints—and they are not substantially weakened by dropping the assumption of spatial flatness. Relaxing the assumption that w is constant and parameterizing its variation as $w(z) = w_0 + w_a(1 - a)$, the current observational constraints are considerably weaker, $\Omega_{DE} \approx 0.7 \pm 0.15$, $w_0 \approx -1 \pm 0.2$, $w_a \approx 0 \pm 1$, and they provide no evidence for variation of w.

10.1.6. Dark theory: dark energy or new gravitational physics? There is no compelling model for dark energy. Beyond vacuum energy, there are many intriguing ideas, including a new light scalar field and the influence of additional spatial dimensions. In many of these models, time-varying dark energy is expected. However, cosmic acceleration could be a manifestation of gravitational physics beyond GR rather than dark energy. Although these suggestions are interesting, there is as yet no self-consistent model for the new gravitational physics that is also consistent with the large body of data that constrains theories of gravity.

10.1.7. Dark destiny. The destiny of the universe depends crucially upon the nature of dark energy. All three fates—recollapse or continued expansion with and without slowing—are possible. The existence of dark energy raises the issue of cosmic uncertainty: Can we determine the mass/energy content with sufficient precision to rule out the possibility that a tiny dark energy component today may dominate in the distant future?

10.1.8. At the nexus of many mysteries. Because of its multiple close connections to important problems in both physics and astronomy, cosmic acceleration may be the most profound mystery in science. Its solution could shed light on or be central to unraveling other important puzzles, including the cause of cosmic inflation, the vacuum energy problem, supersymmetry and superstrings, neutrino mass, new gravitational physics, and even dark matter.

10.1.9. The two big questions. Today, the two most pressing questions about cosmic acceleration are (*a*) Is dark energy something other than vacuum energy? (*b*) Does GR self-consistently describe cosmic acceleration? Establishing that $w \neq -1$, that the value of w varies with time, or that dark energy clusters would rule out vacuum energy. Establishing that the values of w determined by the geometric and growth of structure methods are not equal could point toward a modification of gravity as the cause of accelerated expansion.

10.1.10. Probing dark energy. An impressive array of space- and ground-based observations, using supernovae, weak lensing, clusters, and baryon acoustic oscillations, are in progress or are being planned. They should determine w_p, the equation-of-state parameter at the redshift where it is best determined, at the percent level and its time variation w_a at the 10% level, which would dramatically improve our ability to discriminate between vacuum energy and something more exotic. Such determinations would also test the self-consistency of GR to explain cosmic acceleration. Laboratory- and accelerator-based experiments could also shed light on dark energy.

10.2. Open Issues and Challenges

10.2.1. Clustering of dark energy. Although vacuum energy is uniform, dynamical forms of dark energy can be inhomogeneous, making dark energy clustering a potential additional probe of dark energy. However, because dark energy is likely to cluster only weakly and on the largest scales, the prospects for clustering as a probe of dark energy are not high. Nonetheless, discovering that dark energy does cluster would rule out vacuum energy. Current constraints on the clustering of dark energy are weak, and better ideas about measuring dark energy clustering may be forthcoming.

10.2.2. Dark energy and matter. In scalar-field models of dark energy, there is a new, very light ($m \leq H_0 \sim 10^{-33}$ eV) scalar particle that can couple to matter and thereby give rise to new long-range forces with potentially observable consequences. Such an interaction could perhaps help explain the near-coincidence between the present densities of dark matter and dark energy; it could also change the dynamics of dark matter particles, although it is constrained by astrophysical and cosmological observations to be of at most gravitational strength (Gradwohl & Frieman 1992, Carroll 1998). A coupling to ordinary matter would have even larger observable effects and would be highly constrained.

10.2.3. Describing cosmic acceleration and dark energy. In the absence of theoretical guidance, the equation-of-state parameter $w \equiv p/\rho$ is a convenient way of characterizing dark energy and its effects on cosmic expansion. Alternatively, one can take a more agnostic approach and interpret results in terms of the kinematics of the expansion or the energy density. Further, it is worth exploring improved descriptions of dark energy that both yield physical insight and are better matched to the observations.

10.2.4. Systematic errors. All of the techniques used to probe dark energy are limited by systematic errors. The sources of systematic error include luminosity evolution and dust extinction uncertainties (for SNe Ia); shape measurement systematics, photometric redshift errors, and theoretical modeling of the matter power spectrum (for WL); galaxy biasing, nonlinearity, and redshift distortions (for BAO); and the uncertain relations between cluster mass and its observable proxies (for CL). Improvements in all of these will be critical to realizing the full potential of planned observations to probe dark energy and will have broad beneficial effects in astronomy.

10.2.5. Dark energy theory. The grandest challenge of all is a deeper understanding of the cause of cosmic acceleration. What is called for is not the invention of ad hoc models based upon clever ideas or new potentials, but rather a small number of theoretical models that are well motivated by fundamental physics and that make specific enough predictions to be falsified.

10.2.6. How much is enough? Given its profound implications and the absence of a compelling theory, dark energy is the exemplar of high-risk, high-gain science. Carrying out the most ambitious proposed dark energy projects—JDEM and LSST—to attain percent level precision will cost more than $1 billion. Although they will yield much tighter parameter constraints, there is no guarantee that these projects will deliver a deeper understanding of dark energy. If they are able to exclude vacuum energy or demonstrate the inconsistency of GR, the implications would be revolutionary. However, if they yield results that are consistent with vacuum energy, it would constitute an important test of the null hypothesis and provide a set of cosmological parameters that would satisfy the needs for astrophysical cosmology for the foreseeable future. In this case, unless new theoretical developments pointing to different or more decisive probes of compelling

dark energy theories emerge, there is likely to be little enthusiasm for carrying out even more expensive dark energy projects.

There is no doubt that pursuing the origin of cosmic acceleration will continue to be a great intellectual adventure over the next 15 years. Even if these ambitious projects do not solve this riddle, they will at least help refine the scope of the problem and produce a wealth of survey data that will benefit many areas of astronomy for decades to come.

APPENDIX

A1. Figure(s) of Merit

How do we compare the dark energy "reach" of different methods and different experiments? We cannot quantify the probative power of dark energy methods in a strictly model-independent way, as we do not know which aspects of the expansion history are most important to measure. Nevertheless, some useful figures of merit (FoMs) have been proposed to facilitate comparison of methods and experimental designs. Examples include the volume of the uncertainty ellipsoid for the dark energy parameters and the thickness of the ellipsoid in its narrowest direction (Huterer & Turner 2001). In the Fisher matrix approach (see Section A.2), these FoMs correspond to the inverse square root of the determinant and the largest eigenvalue of the Fisher matrix, respectively. A special case of the volume FoM is the inverse area of the Fisher matrix–projected ellipse in the w_0-w_a plane,

$$\text{FoM} \propto [\sigma(w_0)\sigma(w_a)]^{-1} \propto (\det F^{w_0 w_a})^{1/2} , \qquad (37)$$

where $F^{w_0 w_a}$ is the Fisher matrix projected onto the w_0-w_a plane. This choice was adopted by the DETF as a metric for comparing methods and surveys and is shown in relative terms for Stage IV space-based experiments in **Figure 16**. The DETF FoM provides a simple but useful metric for comparison, as it takes into account the power of experiments to measure the temporal variation of w. For generalizations, see Albrecht & Bernstein (2007).

A2. Fisher Information Matrix

The Fisher information matrix formalism allows a quick and easy way to estimate errors on cosmological parameters, given errors in observable quantities, and it is particularly useful in experimental design. The Fisher matrix is defined as the (negative) Hessian of the log-likelihood function $\mathcal{L}$,

$$F_{ij} \equiv \left\langle -\frac{\partial^2 \ln \mathcal{L}}{\partial p_i \partial p_j} \right\rangle = \mu_{,i}^T \mathbf{C}^{-1} \mu_{,j} + \frac{1}{2}\text{Tr}\left[\mathbf{C}^{-1}\mathbf{C}_{,i}\mathbf{C}^{-1}\mathbf{C}_{,j}\right] . \qquad (38)$$

The second equality follows by assuming that $\mathcal{L}$ is Gaussian in the observables; here μ is the vector of mean values of the observables, $\mathbf{C}$ is their covariance matrix, and $_{,i}$ denotes a derivative with respect to ith model parameter p_i. The parameter vector $\vec{p}$ includes both cosmological and any other model parameters needed to characterize the observations. This expression often simplifies: For example, for N observable quantities with mean values $\mathbf{O}_\alpha$ and a covariance matrix $\mathbf{C}$ that does not depend on the cosmological parameters, the Fisher matrix becomes

$$F_{ij} = \sum_{\alpha,\beta}(\partial \mathbf{O}_\alpha/\partial p_i)\mathbf{C}_{\alpha\beta}^{-1}(\partial \mathbf{O}_\beta/\partial p_j). \qquad (39)$$

By the Cramer-Rao inequality, a model parameter p_i cannot be measured to a precision better than $1/\sqrt{F_{ii}}$, when all other parameters are fixed, or to a precision $\sqrt{F_{ii}^{-1}}$ when all other parameters

are marginalized over. In practice, the Fisher matrix is a good approximation to the uncertainties as long as the likelihood can be approximated by a Gaussian, which is generally the case near the peak of the likelihood and when the parameters are measured with small errors. Conversely, if the errors are large, then the likelihood is typically non-Gaussian, and the constraint region is not elliptical but characteristically banana shaped (**Figure 8**). In this case, the Fisher matrix typically underestimates the true parameter errors and degeneracies, and one should employ a Monte Carlo approach to error estimation.

DISCLOSURE STATEMENT

The authors are not aware of any biases that might be perceived as affecting the objectivity of this review.

LITERATURE CITED

Afshordi N, Loh YS, Strauss MA. 2004. *Phys. Rev. D* 69:083524

Aguirre AN. 1999. *Astrophys. J. Lett.* 512:L19

Albrecht A, Bernstein G. 2007. *Phys. Rev. D* 75:103003

Albrecht A, Bernstein G, Cahn R, Freedman WL, Hewitt J, et al. 2006. (astro-ph/0609591)

Alcock C, Paczynski B. 1979. *Nature* 281:358

Allen SW, Rapetti DA, Schmidt RW, Ebeling H, Morris G, Fabian AC. 2007. *MNRAS* 383:879

Allen SW, Schmidt RW, Ebeling H, Fabian AC, van Speybroeck L. 2004. *MNRAS* 353:457

Alnes H, Amarzguioui M, Gron O. 2006. *Phys. Rev. D* 73:083519

Armendariz-Picon C, Mukhanov VF, Steinhardt PJ. 2000. *Phys. Rev. Lett.* 85:4438

Arnaud M. 2005. In *Background Microwave Radiation and Intracluster Cosmology*, ed. F Melchiorri, Y Rephaeli, p. 77. Bologna: Soc. Ital. Fis.

Arnett WD. 1982. *Astrophys. J.* 253:785

Astier P, Guy J, Regnault N, Pain R, Aubourg E, et al. 2006. *Astron. Astrophys.* 447:31

Bacon DJ, Refregier AR, Ellis RS. 2000. *MNRAS* 318:625

Bean R, Hansen SH, Melchiorri A. 2001. *Phys. Rev. D* 64:103508

Bernstein GM, Jain B. 2004. *Astrophys. J.* 600:17

Blake C, Glazebrook K. 2003. *Astrophys. J.* 594:665

Bondi H, Gold T. 1948. *MNRAS* 108:252

Borgani S. 2006. In *Groups of Galaxies in the Nearby Universe*, ed. I Saviane, VD Ivanov, J Borissova, p. 361, *ESO Astrophys. Symp., Santiago, Chile*

Boughn S, Crittenden R. 2004. *Nature* 427:45

Bousso R, Polchinski J. 2000. *JHEP* 0606:006

Busha MT, Adams FC, Wechsler RH, Evrard AE. 2003. *Astrophys. J.* 596:713

Caldwell RR. 2002. *Phys. Lett. B* 545:23

Caldwell RR, Kamionkowski M, Weinberg NN. 2003. *Phys. Rev. Lett.* 91:071301

Caldwell RR, Linder EV. 2005. *Phys. Rev. Lett.* 95:141301

Carlstrom JE, Holder GP, Reese ED. 2002. *Annu. Rev. Astron. Astrophys.* 40:643

Carroll SM. 1998. *Phys. Rev. Lett.* 81:3067

Carroll SM. 2001. *Living Rev. Relativ.* 4:1

Carroll SM, Duvvuri V, Trodden M, Turner MS. 2004. *Phys. Rev. D* 70:043528

Carroll SM, Hoffman M, Trodden M. 2003. *Phys. Rev. D* 68:023509

Carroll SM, Press WH, Turner EL. 1992. *Annu. Rev. Astron. Astrophys.* 30:499

Chae KH. 2007. *Astrophys. J. Lett.* 658:L71

Chu M, Knox L. 2005. *Astrophys. J.* 620:1

Coble K, Dodelson S, Frieman JA. 1997. *Phys. Rev. D* 55:1851

Cooray A, Huterer D, Baumann D. 2004. *Phys. Rev. D* 69:027301

Copeland EJ, Sami M, Tsujikawa S. 2006. *Int. J. Mod. Phys. D* 15:1753
Corasaniti PS, Copeland EJ. 2003. *Phys. Rev. D* 67:063521
Dalal N, Holz DE, Hughes SA, Jain B. 2006. *Phys. Rev. D* 74:063006
de Sitter W. 1917. *Proc. Natl. Acad. Sci. USA* 19:1217
Deffayet C. 2001. *Phys. Lett. B* 502:199
Dodelson S. 2003. *Modern Cosmology*. Amsterdam: Academic
Doran M, Robbers G. 2006. *JCAP* 0606:026
Drell PS, Loredo TJ, Wasserman I. 2000. *Astrophys. J.* 530:593
Dvali GR, Gabadadze G, Porrati M. 2000. *Phys. Lett. B* 485:208
Efstathiou G, Sutherland WJ, Maddox SJ. 1990. *Nature* 348:705
Einstein A. 1917. *Sitzungsber. K. Akad.* 6:142
Eisenstein DJ, Zehavi I, Hogg DW, Scoccimarro R, Blanton MR, et al. 2005. *Astrophys. J.* 633:560
Enqvist K. 2008. *Gen. Relativ. Gravity* 40:451
Fosalba P, Gaztanaga E. 2004. *MNRAS* 350:L37
Freedman WL, Madore BF, Gibson BK, Ferrarese L, Kelson DD, et al. 2001. *Astrophys. J.* 553:47
Friedman AS, Bloom JS. 2005. *Astrophys. J.* 627:1
Frieman JA, Hill CT, Stebbins A, Waga I. 1995. *Phys. Rev. Lett.* 75:2077
Frieman JA, Huterer D, Linder EV, Turner MS. 2003. *Phys. Rev. D* 67:083505
Fukugita M, Futamase T, Kasai M, Turner EL. 1992. *Astrophys. J.* 393:3
Gamow G. 1970. *My World Line*. New York: Viking
Gerke BF, Efstathiou G. 2002. *MNRAS* 335:33
Gradwohl BA, Frieman JA. 1992. *Astrophys. J.* 398:407
Gregory R, Kaloper N, Myers RC, Padilla A. 2007. *JHEP* 10:069
Guerra EJ, Daly RA, Wan L. 2000. *Astrophys. J.* 544:659
Gunn JE, Tinsley BM. 1975. *Nature* 257:454
Guth AH. 1981. *Phys. Rev. D* 23:347
Guzik J, Bernstein G, Smith RE. 2007. *MNRAS* 375:1329
Haiman Z, Mohr JJ, Holder GP. 2001. *Astrophys. J.* 553:545
Hamuy M, Phillips MM, Suntzeff NB, Schommer RA, Maza J, et al. 1996. *Astron. J.* 112:2408
Hennawi JF, Spergel DN. 2005. *Astrophys. J.* 624:59
Heymans C, White M, Heavens A, Vale C, van Waerbeke L. 2006. *MNRAS* 371:750
Hillebrandt W, Niemeyer JC. 2000. *Annu. Rev. Astron. Astrophys.* 38:191
Hirata CM, Seljak U. 2004. *Phys. Rev. D* 70:063526
Hoeflich P. 2004. In *Supernovae as Cosmological Lighthouses*, ed. M Turatto, S Benetti, L Zampieri, W Shea, *ASP Conf. Ser. Padua, Italy*
Hoekstra H, et al. 2006. *Astrophys. J.* 647:116
Hoyle F. 1948. *MNRAS* 108:372
Hu W. 2002. *Phys. Rev. D* 65:023003
Hu W. 2005. *ASP Conf. Ser.* 339:215
Hu W, Dodelson S. 2002. *Annu. Rev. Astron. Astrophys.* 40:171
Hu W, Haiman Z. 2003. *Phys. Rev. D* 68:063004
Hu W, Holz DE, Vale C. 2007. *Phys. Rev. D* 76:127301
Hu W, Jain B. 2004. *Phys. Rev. D* 70:043009
Hu W, Scranton R. 2004. *Phys. Rev. D* 70:123002
Hubble E. 1929. *Proc. Natl. Acad. Sci. USA* 15:168
Hui L, Greene PB. 2006. *Phys. Rev.* 73:123526
Hui L, Stebbins A, Burles S. 1999. *Astrophys. J. Lett.* 511:L5
Huterer D. 2002. *Phys. Rev. D* 65:063001
Huterer D, Cooray A. 2005. *Phys. Rev. D* 71:023506
Huterer D, Starkman G. 2003. *Phys. Rev. Lett.* 90:031301
Huterer D, Takada M, Bernstein G, Jain B. 2006. *MNRAS* 366:101
Huterer D, Turner MS. 1999. *Phys. Rev. D* 60:081301
Huterer D, Turner MS. 2001. *Phys. Rev. D* 64:123527

Jaffe AH, Ade PA, Balbi A, Bock JJ, Bond JR, et al. 2001. *Phys. Rev. Lett.* 86:3475

Jain B, Taylor A. 2003. *Phys. Rev. Lett.* 91:141302

Jarvis M, Jain B, Bernstein G, Dolney D. 2006. *Astrophys. J.* 644:71

Jha S, Riess AG, Kirshner RP. 2007. *Astrophys. J.* 659:122

Jimenez R, Loeb A. 2002. *Astrophys. J.* 573:37

Johnston DE, Sheldon ES, Wechsler RH, Rozo E, Koester BP, et al. 2008. In press (astro-ph/0709.1159)

Kaiser N. 1992. *Astrophys. J.* 388:272

Kaiser N, Wilson G, Luppino GA. 2000. (astro-ph/0003338)

Kim A. 2004. *LBNL Rep. No. LBNL-56164*

Knop RA, Aldering G, Amanullah R, Astier P, Blanc G, et al. 2003. *Astrophys. J.* 598:102

Knox L, Song YS, Tyson JA. 2006. *Phys. Rev. D* 74:023512

Kochanek CS. 1996. *Astrophys. J.* 466:638

Koester BP, McKay TA, Annis J, Wechsler RH, Evrard A, et al. 2007. *Astrophys. J.* 660:239

Kolb EW, Matarrese S, Riotto A. 2006. *New J. Phys.* 8:322

Kolb EW, Turner MS. 1990. *The Early Universe*. Reading, MA: Addison-Wesley

Kowalski M, Rubin D, Aldering G, Agostinho RJ, Amadon A, et al. 2008. *Ap. J.* In press (astro-ph/0804.4142)

Krauss LM, Chaboyer B. 2003. *Science* 299:65

Krauss LM, Scherrer RJ. 2007. *Gen. Relativ. Gravity* 39:1545

Krauss LM, Turner MS. 1995. *Gen. Relativ. Gravity* 27:1137

Leibundgut B. 2001. *Annu. Rev. Astron. Astrophys.* 39:67–98

Lima M, Hu W. 2004. *Phys. Rev. D* 70:043504

Linder EV. 2003. *Phys. Rev. Lett.* 90:091301

Linder EV. 2008. *Gen. Relativ. Gravity* 40:329

Lue A, Scoccimarro R, Starkman G. 2004. *Phys. Rev. D* 69:044005

Ma Z, Hu W, Huterer D. 2006. *Astrophys. J.* 636:21

Majumdar S, Mohr JJ. 2004. *Astrophys. J.* 613:41

Massey R, et al. 2007. *Nature* 445:286

Meneghetti M, Jain B, Bartelmann M, Dolag K. 2005. *MNRAS* 362:1301

Miknaitis G, et al. 2007. *Astrophys. J.* 666:674

Mitchell JL, Keeton CR, Frieman JA, Sheth RK. 2005. *Astrophys. J.* 622:81

Mohr JJ. 2005. In *Astron. Soc. Pac. Conf. Ser.*, Vol. 339: *Observing Dark Energy*, ed. SC Wolff, TR Lauer, p. 140. San Francisco: Astron. Soc. Pac.

Motl PM, Hallman EJ, Burns JO, Norman ML. 2005. *Astrophys. J. Lett.* 623:L63

Munshi D, Valageas P, Van Waerbeke L, Heavens A. 2008. *Phys. Rep.* 462:67–121

Nagai D. 2006. *Astrophys. J.* 650:538

Nagamine K, Loeb A. 2003. *New Astronomy* 8:439

Nakamura T, Chiba T. 1999. *MNRAS* 306:696

Ostriker JP, Steinhardt PJ. 1995. *Nature* 377:600

Padmanabhan T. 2003. *Phys. Rept.* 380:235

Peacock JA. 1999. *Cosmological Physics*. Cambridge, UK: Cambridge Univ. Press

Peebles PJE. 1984. *Astrophys. J.* 284:439

Peebles PJE. 1993. *Principles of Physical Cosmology*. Princeton: Princeton Univ. Press

Peebles PJE, Ratra B. 2003. *Rev. Mod. Phys.* 75:559

Perlmutter S, Aldering G, Goldhaber G, Knop RA, Nugent P, et al. 1999. *Astrophys. J.* 517:565

Perlmutter S, Gabi S, Goldhaber G, Goobar A, Groom DE, et al. 1997. *Astrophys. J.* 483:565

Perlmutter S, Schmidt BP. 2003. In *Lect. Notes Phys.*, Vol. 598: *Supernovae and Gamma-Ray Bursters*, ed. K Weiler, pp. 195–217. Berlin: Springer-Verlag

Petrosian V, Salpeter E, Szekeres P. 1967. *Astrophys. J.* 147:1222

Phillips MM. 1993. *Astrophys. J. Lett.* 413:L105

Plewa T, Calder AC, Lamb DQ. 2004. *Astrophys. J. Lett.* 612:L37

Pryke C, Halverson NW, Leitch EM, Kovac J, Carlstrom JE, et al. 2002. *Astrophys. J.* 568:46

Rapetti D, Allen SW, Mantz A. 2008. *MNRAS* In press (astro-ph/0710.0440)

Rapetti D, Allen SW, Amin MA, Blandford RD. 2007. *MNRAS* 375:1510

Ratra B, Peebles PJE. 1988. *Phys. Rev. D* 37:3406

Reichardt CL, Ade PAR, Bock JJ, Bond JR, Brevik JA, et al. 2008. (astro-ph/0801.1491)

Riess AG. 2000. *Pub. Astron. Soc. Pac.* 112:1284

Riess AG, Filippenko AV, Challis P, Clocchiatti A, Diercks A, et al. 1998. *Astron. J.* 116:1009

Riess AG, Nugent PE, Gilliland RL, Schmidt BP, Tonry J, et al. 2001. *Astrophys. J.* 560:49

Riess AG, Strolger LG, Casertano S, Ferguson HC, Mobasher B, et al. 2007. *Astrophys. J.* 659:98

Riess AG, Strolger LG, Tonry J, Casertano S, Ferguson HC, et al. 2004. *Astrophys. J.* 607:665

Sahni V, Starobinsky A. 2006. *Int. J. Mod. Phys. D* 15:2105

Sandage A. 1962. *Astrophys. J.* 136:319

Sandage AR. 1970. *Phys. Today* 23:34

Schaefer BE. 2003. *Astrophys. J. Lett.* 583:L67

Schneider P. 2006. In *Saas-Fee Adv. Course*, Vol. 33: *Gravitational Lensing: Strong, Weak and Micro*, ed. G Meylan, P Jetzer, P North, P Schneider, CS Kochanek, J Wambsganss, pp. 1–89. Berlin: Springer

Scranton R, Connolly AJ, Nichol RC, Stebbins A, Szapudi I, et al. 2003. (astro-ph/0307335)

Seo HJ, Eisenstein DJ. 2003. *Astrophys. J.* 598:720

Seo HJ, Eisenstein DJ. 2007. *Astrophys. J.* 665:14

Shapiro C, Turner MS. 2006. *Astrophys. J.* 649:563

Smith RE, Scoccimarro R, Sheth RK. 2007. *Phys. Rev. D* 77:043525

Song YS, Hu W, Sawicki I. 2007. *Phys. Rev. D* 75:044004

Spergel DN, Bean R, Doré O, Nolta MR, Bennett CL, et al. 2007. *Astrophys. J. Suppl.* 170:377

Springel V, Frenk CS, White SDM. 2006. *Nature* 440:1137

Stanek R, Evrard AE, Bohringer HB, Schuecker P, Nord B. 2006. *Astrophys. J.* 648:956

Starobinsky AA. 1998. *JETP Lett.* 68:757

Straumann N. 2002. (gr-qc/0208027)

Sunyaev RA, Zeldovich YB. 1970. *Comments Astrophys. Space Phys.* 2:66

Susskind L. 2007. In *Universe or Multiverse?*, ed. B Carr, pp. 247–66. Cambridge, UK: Cambridge Univ. Press

Takada M, Jain B. 2004. *MNRAS* 348:897

Tegmark M, Eisenstein DJ, Strauss MA, Weinberg DH, Blanton MR, et al. 2006. *Phys. Rev. D* 74:123507

Tinsley BM, Gunn JE. 1976. *Astrophys. J.* 203:52

Tomita K. 2001. *MNRAS* 326:287

Turner MS. 1991. In *Astrophys. Space. Sci. Libr.*, Vol. 169: *Primordial Nucleosynthesis and Evolution of the Early Universe*, ed. K Sato, J Audouze, pp. 337–50, *Proc. Int. Conf.*, *Univ. Tokyo*, *Japan*

Turner MS, Steigman G, Krauss LM. 1984. *Phys. Rev. Lett.* 52:2090

Turner MS, White MJ. 1997. *Phys. Rev. D* 56:4439

Turok N, ed. 1997. *Critical Dialogues in Cosmology*. Singapore: World Scientific

Uzan JP. 2007. *Gen. Relativ. Gravity* 39:307

Van Waerbeke L, Mellier Y, Erben T, Cuillandre JC, Bernardeau F, et al. 2000. *Astron. Astrophys.* 358:30

Visser M. 2004. *Class. Quant. Gravity* 21:2603

Wang L, Steinhardt PJ. 1998. *Astrophys. J.* 508:483

Wang S, Hui L, May M, Haiman Z. 2007. *Phys. Rev. D* 76:063503

Wang Y, Mukherjee P. 2004. *Astrophys. J.* 606:654

Warren MS, Abazajian K, Holz DE, Teodoro L. 2006. *Astrophys. J.* 646:881

Weinberg S. 1987. *Phys. Rev. Lett.* 59:2607

Weinberg S. 1989. *Rev. Mod. Phys.* 61:1

Weller J, Albrecht A. 2002. *Phys. Rev. D* 65:103512

Wetterich C. 1988. *Nucl. Phys. B* 302:668

White M, van Waerbeke L, Mackey J. 2002. *Astrophys. J.* 575:640

Wittman DM, Tyson JA, Kirkman D, Dell'Antonio I, Bernstein G. 2000. *Nature* 405:143

Wood-Vasey WM, Miknaitis G, Stubbs CW, Jha S, Riess AG, et al. 2007. *Astrophys. J.* 666:694

Yee HKC, Gladders MD. 2002. In *Astron. Soc. Pac. Conf. Ser.*, Vol. 257: *AMiBA 2001. High-Z Clusters, Missing Baryons, and CMB Polarization*, ed. LW Chen, CP Ma, KW Ng, UL Pen, p. 109. San Francisco: Astron. Soc. Pac.

Zel'dovich YB. 1968. *Sov. Phys. Usp.* 11:381

Zentner AR, Rudd DH, Hu W. 2007. *Phys. Rev. D* 77:043507

Zlatev I, Wang LM, Steinhardt PJ. 1999. *Phys. Rev. Lett.* 82:896

Contents

Indexes

Errata

An online log of corrections to *Annual Review of Astronomy and Astrophysics* articles may
be found at http://astro.annualreviews.org/errata.shtml